FACULDADE DE ENGENHARIA DA UNIVERSIDADE DO PORTO

Hydrodynamic Improvements Of A Stern Foil For A 120 feet Solar Powered Catamaran With Subcritical Flows Through CFD Analysis

Vasco Mimoso Luís

Masters in Mechanical Engineering, Specialization in Fluids and Energy

Supervisor: Prof. Abel Roboa, FEUP

Second Supervisor: Dr. Stephan Kress, Silent Yachts

October 10, 2023

Hydrodynamic Improvements Of A Stern Foil For A 120 feet Solar Powered Catamaran With Subcritical Flows Through CFD Analysis

Vasco Mimoso Luís

Masters in Mechanical Engineering, Specialization in Fluids and Energy

October 10, 2023

Abstract

The primary purpose of this thesis was to improve the hydrodynamic performance of the super yacht Silent 120. Since the design of the vessel was already established along with its components, only appendix like additions could be made to the hull, which could take form as trim correction flaps, lift generating foils, protuberances for vortex generation, among others. Between all of the options the lift generating foils were by far the most popular choice in the naval industry, not only did they improve tremendously the seakeeping ability of the vessel in question, they allowed for the greatest resistance reduction out of all of the possible alternatives; dued to their simple complexity, they enabled easy implementation to an array of different scenarios. In our case of a full displacement vessel this meant the form of a stern foil.

In order to predict the perfomance of the vessel, computational fluid dynamic simulations were performed. To do so accurately a 2 dimensional validation scenario was applied, where the aim was to recreate experimental simulations done to an hydrofoil, in a computational manner. In doing so we would be able to minimize the error associated with the computational solver.

Once the error achieved an acceptable level came the choice of the hydrofoil profile for the stern foil. Since the choices were far too vast to be all analyzed, only the already studied profiles from the literature were taken into account, with a few exceptions. In order to determine the best profile to use, a 2 dimensional comparison was done, in which the NACA 6418 proved to be the best fit.

Finally, came the choice of the positioning of the stern foil. Here, yet again, a 2 dimensional simulation was performed with the vessel and the stern foil in several different positions, and only after acquiring the ideal positioning did we conduct a 3 dimensional simulation to acquire the final results; these included the vessel in its simplest form and the hull with the added stern foil; dued to a lack in computational power these results are yet to be obtained.

Resumo

O objetivo principal desta tese foi melhorar o desempenho hidrodinâmico do super iate Silent 120. Como o projeto da embarcação já estava estabelecido junto com seus componentes, apenas adições semelhantes a apêndices poderiam ser feitas ao casco, que poderiam assumir a forma de "Trim correction flaps", "lift generating foils", "protuberances for vortex generation", entre outros. Entre todas as opções, as "lift generating foils" foram de longe a escolha mais popular na indústria naval, não só melhoraram tremendamente a capacidade de navegação do navio em questão, como permitiram a maior redução de resistência de todas as alternativas possíveis; devido à sua simples complexidade , elas permitiam fácil implementação numa variedade de cenários diferentes. No nosso caso de uma embarcação de "fully displacement", isso significava a forma de um "stern foil".

Para prever o desempenho da embarcação, foram realizadas simulações computacionais de dinâmica de fluidos. Para fazê-lo com precisão foi aplicado um cenário de validação bidimensional, onde o objetivo era recriar simulações experimentais feitas com um "hydrofoil", de forma computacional. Ao fazer isso, seríamos capazes de minimizar o erro associado ao programa computacional.

Uma vez atingido um erro aceitável, veio a escolha do perfil do "hydrofoil" para o "stern foil". Dado que as escolhas eram demasiado vastas para serem todas analisadas, apenas foram tidos em conta os perfis já estudados na literatura, com algumas excepções. Para determinar o melhor perfil a utilizar foi feita uma comparação bidimensional, na qual o NACA 6418 revelou-se ser o melhor ajuste.

Por fim, veio a escolha do posicionamento do "stern foil". Aqui, mais uma vez, foi realizada uma simulação bidimensional com a embarcação e o "stern foil" em diversas posições diferentes, e somente após adquirir o posicionamento ideal é que procedemos para uma simulação tridimensional para adquirir os resultados finais; estes incluíam o casco na sua forma mais simples e o casco com o "stern foil" adicionado; devido à falta de poder computacional, esses resultados ainda não foram obtidos.

Acknowledgements

I'm very thankful to Silent Yachts for allowing me to be apart of such an amazing company for my master thesis.

To the incredible team in Mallorca, I express my thanks for the warm welcome and for helping me along this study.

To my supervisor, Prof. Abel Roboua, I'd like to thank you for all of the devoted support and patience.

A special thanks to the Naval Eng. Miguel Rigo for being always ready to help and for guiding me through the problems we encountered, without your help this thesis wouldn't have been what it is.

To PhD Stephan Kress I can only express my upmost gratitude since without your efforts this intership wouldn't have been possible, thank you.

And finally, many thanks to my family and friends for being understanding and supporting throughout this incredible step of my life.

Vasco Mimoso Luís

'We cannot solve problems with the kind of thinking we employed when we came up with them."

Albert Einstein

Contents

List of Figures

List of Tables

Nomenclature

AoA	Angle of Attack
BoI	Body of Influence
Cl	Chord length
HYSUCAT	HYdrofoil SUported CATamaran
Hl	Hull length
HV	Hull Vane®
Lwl	Levelized water line
NACA	National Advisory Committee for Aeronautics
RANS	Reynolds Averaged Navier-Stokes
SY120	Silent Yacht 120
UDF	User-Defined Function
VoF	Volume of Fluid

Symbols

α	Angle of Attack	[rad]
β	Hull Vane® angle	[rad]
c	chord length	[m]
C_D	Drag coefficient, $C_d = \frac{D}{\rho V^2 c}$	[-]
C_L	Lift coefficient, $C_l = \frac{L}{\rho V^2 c}$	[-]
$\tilde{C}_{L,Error}$	Average coefficient of lift error	[-]
$\tilde{C}_{D,Error}$	Average coefficient of drag error	[-]
δ	Displacement	[m^3]
D	Drag Force	[N]
D_{HV}	Drag force on the hull vane	[N]
Fn	Froud number, $Fn = \frac{v}{\sqrt{g*Lwl}}$	[-]
F_{HV}	Resulting force on the hull vane	[N]
$F_{x,HV}$	Decomposed resulting force on the hull vane on the x axis	[N]
$F_{z,HV}$	Decomposed resulting force on the hull vane on the z axis	[N]
g	Gravitational constant	[kg.m/s^2]
GM_L	Longitudinal metacentric high	[m]
H_w	Wave height	[m]
I_{xx}	Inertia tensor on the x axis	[kg.m^2]
I_{yy}	Inertia tensor on the y axis	[kg.m^2]
I_{zz}	Inertia tensor on the z axis	[kg.m^2]
L	Lift Force	[N]
L_{HV}	Lift force on the hull vane	[N]
μ	Dynamic viscosity	[Pa.s]
ν	Kinematic viscosity of the fluid	[J.s/kg]
R_T	Total resistance	[N]
ρ	Flow density	[kg/m^3]
θ	Trim angle	[rad]
V	Uniform flow velocity	[m/s]

Chapter 1

Introduction

Companies in the yachting industry must be in constant improvement in order to remain competitive in the market. In their pursuit for excellence Silent Yachts have already revolutionized the way luxury yachts are portrayed, not only can they provide unlimited range but doing so without any emissions. By taking advantage of the most abundant power source, the sun, their solar powered electric yachts replace the vibrations, smell and noise of the combustion engine with the quiet and more efficient electric motor.

This study aims to keep this innovative mentality in mind with the focus of improving the hydrodynamic performance of the vessel. By reducing overall drag, the company can improve on their performance figures hence broadening their potential clients. In order to achieve this goal the idea of implementing an hydrofoil came to light, not only was this a simple implementation but the potential benefits were far too great to ignore. Even though this concept wasn't new to catamarans, HYSUCATs (Hydrofoil Suported Catamarans), the operational speeds required for the hydrofoil to work in this scenario were far too great, this posed an obvious obstacle which demanded an alternative. Still convinced a hydrofoil was the right way to proceed, we turned our attention towards a different application of a hydrofoil, a stern foil or, more commonly known, in the naval industry, as a hull vane. As the name implies the hydrofoil was now installed in the stern of the vessel and not in the conventional place, in between the two hulls. Usually in the scenario of a HYSUCAT, for a fast enough speed, the objective of this installment is to provide enough lift to remove a big percentage of the hull out of the water, this was, however, an impossible task given that our vessels in analysis were fully displacement catamarans with low operational speeds. In our case the sole purpose of the stern foil is to mainly reduce the wave generation at the stern and improve the trim line, thus reducing the energy dissipation of the turbulent flow allowing for an improved and more stable movement through the water.

1.1 The Company

Silent Yachts is a company that specializes in designing and building luxury yachts that can run entirely on solar power. They are the first and only producer of ocean-going solar-electric catamarans in the world. The company was founded in 2009 by Michael Köhler with a vision to create sustainable and environmentally-friendly yachts that don't compromise on luxury nor on an enjoyable experience.

Silent Yachts currently offers various models of solar-electric catamarans, ranging in size from 60, 80 and 120 feet in length along with their variants. These yachts are equipped with solar panels that generate all the energy needed to power the onboard appliances, propulsion, and auxiliary systems. The yachts also come with state-of-the-art technology and luxury features, such as spacious living areas, high-end utilities, and customizable interior designs.

The company has received numerous awards and accolades for their innovative designs and commitment to sustainability. They are leading the way in the yachting industry's transition towards more sustainable and environmentally-friendly practices.

Figure 1.1: The Silent yachts currently in production, the Silent 60, the Silent 80 and the Silent 120, respectively [1].

1.2 The State of The Art

1.2.1 Methods

The Preferred Reporting Items for Systematic Reviews and Meta-Analyses (PRISMA) [2] statement standards were followed for this review.

Initially, for this collection of information a 10 year gap was considerred, when searching for the component "hull vane" and "stern foil", these specifications made little difference since the amount of documentation on this specific installation was very scarce with only english documents being taken into account. In other to gather the most amount of information, three searches were performed, the first with the specific keywords "hull vane", "stern foil", and "t-foil", followed by a search with the more generic keywords "hydrofoil" and "catamaran", and finally "hydrofoil profile" and "stern foil profile", in three different bibliographic databases: *INSPEC*, *SCOPUS*, and *Academic Search Ultimate*.

1. INSPEC (Elsevier-Engineering Village)
    - "(hull vane OR sternfoil) AND (catamaran)"
    - "(hydrofoil) AND (catamaran)"
    - "(hydrofoil profile) AND (stern foil profile)"
2. Academic Search Ultimate
    - "(hull vane OR sternfoil) AND (catamaran)"
    - "(hydrofoil) AND (catamaran)"
    - "(hydrofoil profile) AND (stern foil profile)"
3. Scopus
    - "TITLE-ABS-KEY (hydrofoil AND catamaran) AND PUBYEAR > 2012 AND PUBYEAR < 2024 AND (LIMIT-TO (SUBJAREA , "ENGI")) AND (LIMIT-TO (LANGUAGE , "English"))"
    - "TITLE-ABS-KEY (hull AND vane OR stern AND foil OR t-foil)"
    - "TITLE-ABS-KEY (hydrofoil profile OR stern foil profile)"

Selected articles from each database were exported for screening. Both title and abstract were first examined. Then, with the established selection criteria, full-text articles were retrieved and assessed. In each database, after the combination of keywords was inserted, the following exclusion criteria were applied through search filters:

- Subject Area: Engineering
- Language: English

- Date: Articles published between 2013 and 2023
- Document Type: All
- Source Type: Journal

Upon applying the previous search criteria and removing the duplicated articles we're left with a group of articles that are on topic. However, not all applications of the component were regarding the reduction of the hull resistance, so the articles that focused on the following topics were also excluded:

- Focus on passenger comfort
- Focus on reduction of pitch and heave motion
- Focus on reduction of slamming effects
- Focus on motion controlling

Once the irrelevant articles were removed, the remaining articles could be fully analyzed. During this analysis and to better understand the challenges ahead, the following questions had to be addressed:

- Which are the potential benefits?
- What are the ideal applications?
- Which is the required ideal Froudee number?
- Where is the ideal positioning in terms of depth and distance relative to the stern?
- Which is the ideal shape and size that this stern foil should have?

1.2.2 Selected Articles

The selection of studies was summarised in the PRISMA flow diagram, Figure 1.2 . Three categories were formed, the first regarding the influence of the hull vane, stern foil or t-foil on the hull resistance of multiple ships, particularly not catamarans, for an array of Froudee numbers: [15], [16], [5], [12], [11], [17], [18], [13], [19], [20]. The second category regarded the profile of the stern foil in ways to optimize its shape, compare diferent pre-determined dimensions and other characteristics. Several articles were acquired in order to choose the ideal profile for our scenario: [21], [22], [23], [3], [24], [9], [25], [8], [7], [26], [27], [28], [10], [14]. And the final category involved the studies of hydrofoils in catamarans, unfortunately this category didn't prove to be as useful as it was previously thought. Besides the use of various scenarios, the positioning, shape and amount of these hydrofoils were far too diferent for our study, so only the similar applications were considered: [29], [30], [31],[32]. Some articles didn't belong to any of the above categories, since they constituted regulations, guides and other forms of information unrelated to the stern foil. [2], [33],[34] and [35].

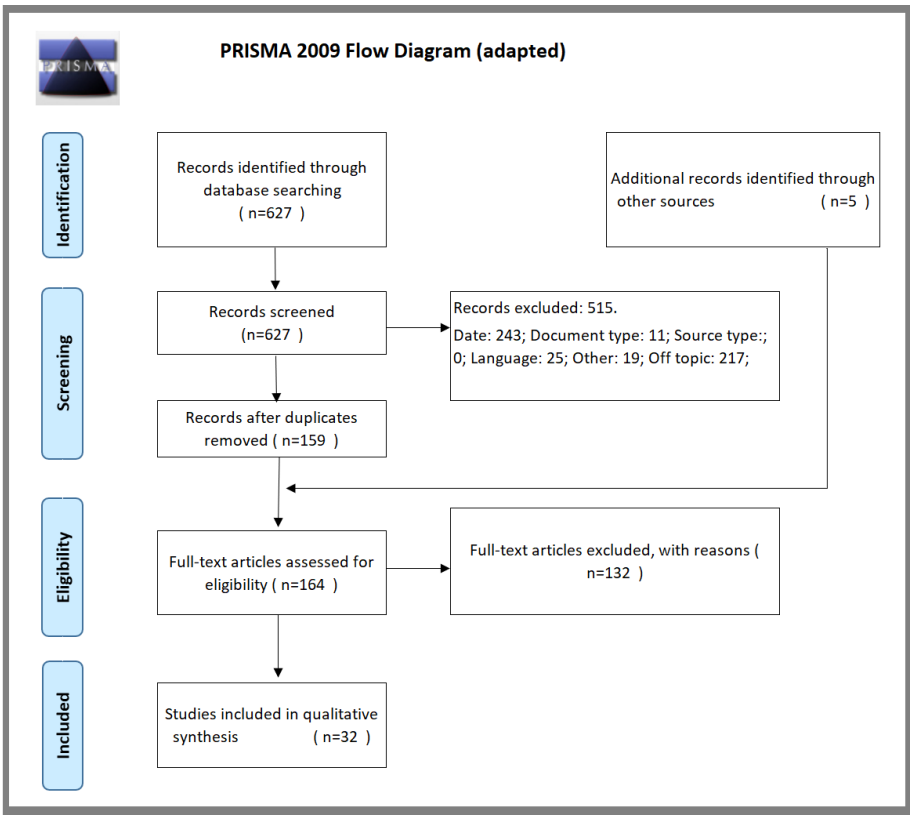

Figure 1.2: PRISMA Flow Diagram, [2].

1.2.3 Findings

Stern Foil

The stern foil was introduced into the naval industry as the patented component and more commonly known Hull Vane® (HV). The HV is an energy-saving appendage introduced by Hull Vane B.V. company to reduce total ship resistance. There have been studies conducted by the inventors, [23], [17], [5] and [15] however, mostly kept confidential; therefore, no detailed research on the design and profile of HV is available in the literature. So for the purpose of this thesis we will use the generic term of stern foil, since this study doesn't have the dimensions of the HV.

In the following figure 1.3 we can observe the angle of attack (AoA) of a normal hydrofoil in order to generate lift, however since the placement of the stern foil, as the name suggests, is at the stern, after the transom of the vessel, the direction of the flow no longer takes an horizontal direction, this causes the AoA of the stern foil to almost take a horizontal like position, as shown in the next figure 1.5. As it can be seen the produced lift force can now generation of a thrust force, equation 1.2, which can compensate or even overcome the produced drag force of the stern foil, which is unusal for an hydrofoil vessel, [5], [18]

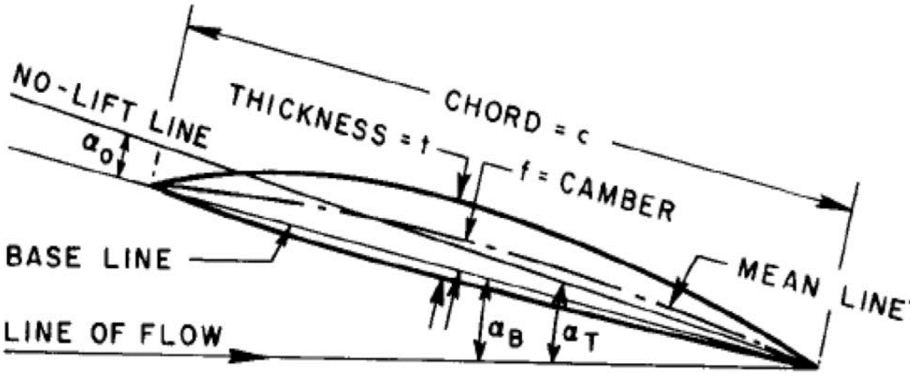

Figure 1.3: Hydrofoil section geometry, [3].

Besides the thrust force, the lift generated will have a greater impact on the total resistence of the vessel, since this vertical force will induce a trim correction, equation 1.4, meaning the vessel will sail with a more horizontal profile which will in turn reduce sinkage and wave generation. Also, since this hydrofoil acts as a barrier to vertical movements the reducion of the pitch and heave motions can be observed, specially in wavy conditions, these benefits, unfortunately, won't be analysed in this study.

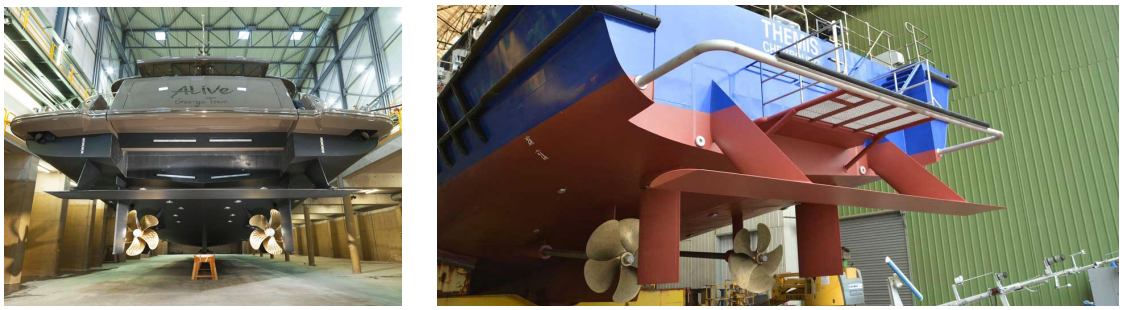

Figure 1.4: Examples of already in used applications of the hull vane, [4].

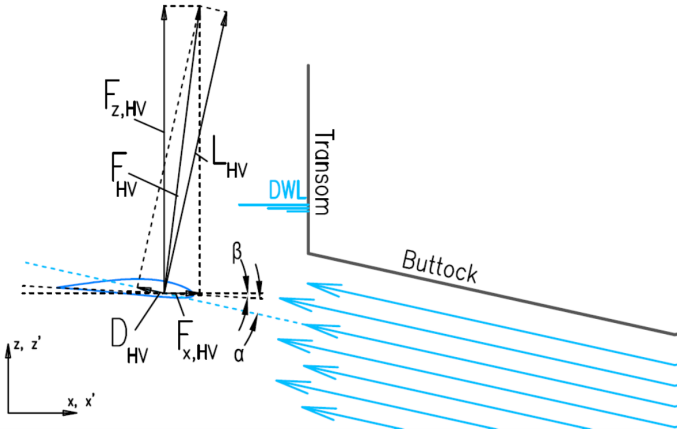

Figure 1.5: The resulting forces acting on the stern foil, [5].

- Force balance on the stern foil, [5]:

$$\vec{L}_{HV} + \vec{D}_{HV} = \vec{F}_{HV} = \vec{F}_{x,HV} + \vec{F}_{z,HV} \tag{1.1}$$

- Thrust force equation, $\vec{F}_{x,HV}$, [5]

$$F_{x,HV} = sin(\alpha + \beta + \theta) * L_{HV} - cos(\alpha + \beta + \theta) * D_{HV} \tag{1.2}$$

- Trim correction equation, [5]:

$$F_{z,HV} = cos(\alpha + \beta + \theta) * L_{HV} + sin(\alpha + \beta + \theta) * D_{HV} \tag{1.3}$$

$$\delta\theta = \frac{\text{trimming moment}}{\text{righting moment per degree of trim}} \approx \frac{F_{z,HV} * \text{arm}}{GM_L * \Delta * g * sin(1)} \tag{1.4}$$

As it is known this generated lift occurs dued to the creation of a low pressure zone on the upper surface of the hydrofoil. As a result, the location of the stern foil is critical in order to properly achieve the benefits. In almost every article acquired the best reported position was behind the transom of the vessel, in an appended fashion, with the ideal positioning taking place around one chord length from the water line and around two to three chord lengths from the transom of the vessel, [5], [16], [22], [17], [11], [12]

In terms of reduction of total resistance, even though all of the articles that analysed the effect of the stern foil/hull vane were displacement monohulls, with the exception of [30], which was the only application of a stern foil in a catamaran, there was a big variety in terms of size, flow velocity, Froudee numbers and hydrofoil profiles. This implied a huge range of different results. From a 10% increase in total resistance for a Froudee number of 0.2 in a 42m motor yacht, [5] to staggering 45% decrease in total resistance for a Froudee number of 0.22 in a 61m patrol boat, [20].

Despite the wide range of applications and study circumstances, almost every article reached the same result. The optimal Froude number, equation 1.5 for the greatest overall resistance decrease was between 0.2 and 0.7, with an emphasis, in most cases, between 0.3 and 0.4. [5],[20],[16],[15], [17], [18], [23]. It´s important to note that for this simulation the Froude number becomes the fundamental value for categorizing the flow. Since we now have an open channel flow, which is heavily influenced by the gravitational forces, the balance between the inertial forces and the gravitational forces becomes much more predominant in describing the type of flow, and thus, the Froude number is used; nevertheless, the balance of the inertial forces with the viscous forces that the Reynolds number categorizes still has importance, in order to predict if the flow is between the a laminar or turbulent state.

$$Fn = \frac{V}{\sqrt{g * Lwl}} \tag{1.5}$$

Hydrofoil Profile

Throughout the years there have been countless introductions of new hydrofoils into the market, so determining the best one for this scenario was a priority since the hydrofoil performance varied immensely with each testing condition. The parameters seen, in figure 1.3, categorize the hydrofoil and are the variables that distinguish the testing conditions from one hydrofoil to another.

From all the studies that aproached the question of finding the best lift to drag ratio, the general conclusion was that in order to obtain the best ratio, the AoA had to be between the values of 2.5º and 8º, [3], [24], [9], [26], [8], [25], [19], [23].

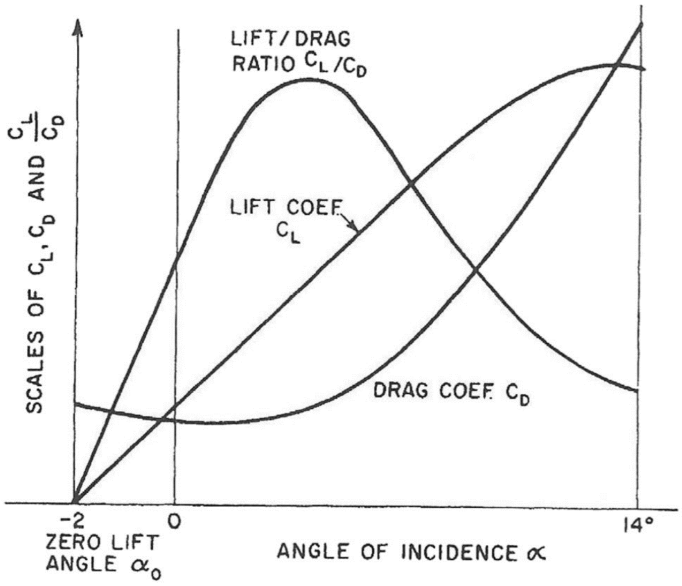

Figure 1.6: Behaviour of the lift and drag coeficients with the AoA, [3].

Besides having found the ideal AoA interval, some articles also touched upon the submergence depth of operation, where the drag and lift coefficients, C_d, C_l respectively in equation 1.6 and equation 1.7, where evaluated for different working depths. It was discovered that with the increase in submergence depth beyond one chord length, the values of the lift and drag coefficients of the hydrofoil would gradually decreased; [9], [10]

$$C_d = \frac{D}{\rho V^2 c} \tag{1.6}$$

$$C_l = \frac{L}{\rho V^2 c} \tag{1.7}$$

Amongst all the possible profiles, and in order to simplify the selection, only the National Advisory Committee for Aeronautics (NACA) profiles were considered. From the NACA profile database the listed profiles, in table 1.1 were the most studied and had the most successful results, in appendix A you can find the hydrofoils with their geometry and profile in more detail. The NACA 4409 and the 6418 were added even though they hadn't been studied before, since one had a different profile from the ones previously studied and the other a smaller value for chord thickness, this allowed for a good comparison between the effects of the chord thickness.

Table 1.1: Listing of the considered hydrofoil profiles

Name	Reference
NACA 0012	[7], [8]
NACA 0018	[8]
NACA 2412	[8]
NACA 4409	-
NACA 4412	[9], [10], [11], [12], [13]
NACA 4418	[14]
NACA 6418	-

It is important to note that the numbers that categorize each hydrofoil mean the following: The first number represents the percentage of the max camber at the second number* 10 chord percentage and the last two numbers represent the max thickness percentage at around 30% chord percentage. For example the NACA 6418:

- 6% max camber at 40% chord length
- 18% max thickness at 30% chord length

Hydrofoil Supported Catamarans

One of the most common hulls is the catamaran. This type of vessel is known by two separate hulls (each of them is called a half-hull) and a deck that connects these. These vessels tend to have large deck area and appropriate transverse stability. Also, they have softer and more comfortable motions during seafaring through waves.

Using hydrofoils between the two hulls of catamarans, an hydrofoil supported catamaran (HYSUCAT), is one of the best ways to improve the hydrodynamic characteristics of these vessels. In almost every single application we would have the main hydrofoil near the center of mass and two, considerably smaller, supporting hydrofoils near the stern of the vessel. The reported results varied between 12% and 36% in drag reduction from speeds of 10 m/s to 20 m/s, respectively, [32], and, a 9% to 14% drag reduction at different velocities for [31]. Finally, with the focus on reducing the wake wash produced by the motions of the vessel, a hydrofoil was installed at the stern of the catamaran; with a great amount of variety in setups, the total resisstance, trim and sinkage was evaluated for different angles of attack (AoA), [30].

It is important to note that most applications revolved around high Froude numbers, equation 1.5, were the vessels in question were planning or semi-planning catamarans. This means the displaced weigth would be in constant change throughout the variation in velocity.

Figure 1.7: Example of an already used application of hydrofoils in catamarans, [6].

1.3 Motivation

Despite the success of their vessels, Silent Yachts recognizes that there is always room for innovation. With this in mind, they presented to me an optimization challenge involving their vessels, with the goal of enhancing the customers autonomy in the open seas.

The Silent Yachts are able to have endless range given that the solar panels can provide all of the energy necessary, however, this is only true if the vessel remains under a speed of 5 to 6 knots, and, as can be expected, if sunlight is present. Above these speeds the generator needs to be used in order to fulfil the energy demands. The usage of the generator is fairly common since the majority of clients prefer to cruise faster than 5 knots. In light of this, Silent Yachts strive to make their product as efficient as possible in order to reduce the need for the generator.

1.4 Objectives

Minimizing the total resistance force of the vessel is the primary goal by default, however improved stability and seakeeping abilities come as secondary consequences of the installation of a stern foil. In order to determine the optimal course of action, changes were made to the hull's design and the shape of its combined components.

The goal of this analysis is to propose the required adjustments in order to produce the most optimal scenario compatible with the company's vision. The best possible stern foil will be designed and displayed here with the help of 2D and 3D modeling and CFD simulations. The obtained results will be presented as the autonomy gained.

Chapter 2

Materials And Methods

In this section will be presented a brief description of the vessel used for generating the test subjects, as well as the dimensions of the hydrofoils which were then imported into *ANSYS (Fluent)* for the computational fluid dynamic (CFD) simulations.

2.1 The Silent Yacht 120

With an impressive length of 120 feet (approximately 36.58 meters), this magnificent catamaran embodies space, elegance, and innovation. True to the Silent Yachts' philosophy, the Silent 120 harnesses the power of the sun to deliver a near silent and emission-free cruising experience. Solar panels gracefully integrated into the yacht's sleek and modern design provide an abundance of clean energy to power its electric propulsion and onboard systems.

The Silent 120 boasts exceptional performance, allowing for extended journeys without the need for fuel as a traditional yacht of its size. Thanks to its advanced solar and battery system, the yacht offers extended range and ensures a smooth, quiet, and vibration-free cruise. With a focus on sustainability, the Silent 120 not only minimizes its impact on the environment but also maximizes your enjoyment of the journey.

In summary, the Silent 120 from Silent Yachts represents the epitome of eco-conscious luxury cruising, where innovation, elegance, and environmental responsibility merge into a single extraordinary yacht. As technology advances and sustainability becomes ever more important, the Silent 120 stands ready to lead the way into a greener and more serene future for yachting enthusiasts worldwide.

Figure 2.1: Silent 120 stern view, [1].

Figure 2.2: Silent 120 bow view, [1].

Surprisingly, the Silent 120 was not the first selection for this study, in fact, out of the three yachts the smallest of the available vessels, the Silent 60, was the most suited, theory wise. It could achieve relatively the same speeds of the other two while having a much smaller length and weight. In terms of froud numbers this was the one that could prove to benefit the most from the addition of a stern foil.

Unfortunately, the hull design of the Silent 60 was flawed for such an application. For a stern foil to work properly the vessel must sail under a displacement hull, meaning as the speed increases the displaced volume remains the same. Both the Silent 60 and Silent 80 had a semi-displacement

hull designs which meant they wouldn't benefit with a stern foil, only the Silent 120 gathered the essential conditions. In the next figure 2.3 a visual representation of the difference between the two hull types can be seen at the stern, where the displacement hull of the Silent 120 has a steeper flow angle compared to the Silent 60.

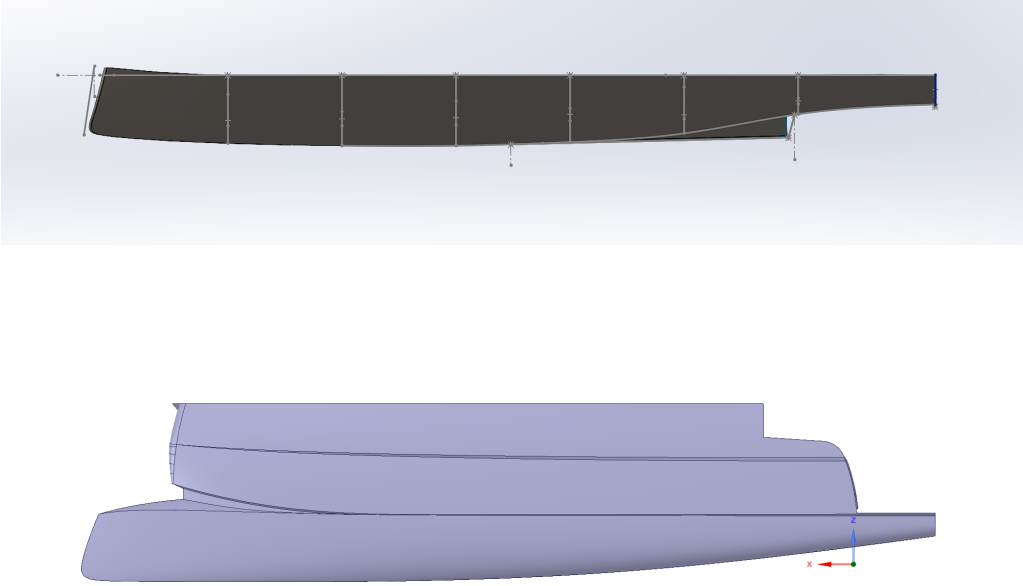

Figure 2.3: Semi-displacement hull of the Silent 60 and the displacement hull of the Silent 120, respectively.

Dimensions and Specifications

Silent Yachts already had a 3D model of the vessel, however, the software used was *Rhino* which wasn't ideal for importing files into *ANSYS* since too many gaps formed in the transition. So a 3D model in *SOLIDWORKS* was made. To reduce computational power and unnecessary meshing elements, only the lower half was recreated. Figures 2.4, 2.5 and 2.6 show the various angles of the 3D vessel.

Figure 2.4: Bow and stern view of the Silent 120 3D model, respectively.

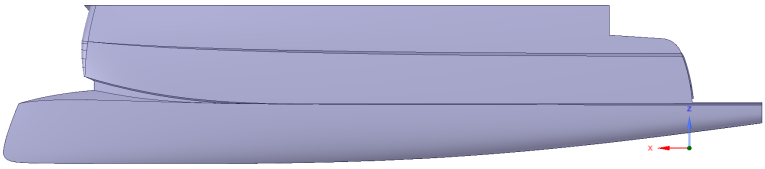

Figure 2.5: Profile view of the SY120 hull.

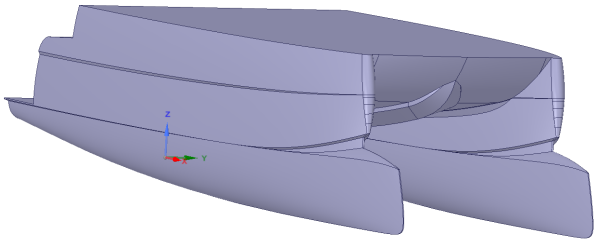

Figure 2.6: Angled view of the SY120 hull.

Table 2.1: Dimensions and specifications of the vessel components

Length [m]	36.74
Beam [m]	13.85
Draft [m]	2.00
Generator [kw]	6x145
Engines [kw]	4x340
Weight[kg]	260000
Top Speed [knots]	12
Max. Froude	0.3523
Total Solar Power [kwp]	40
Total Solar Panel Area [m^2]	100

Hydrofoils

In order to generate the hydrofoils a total of 200 points were imported to create the geometry, these points were obtained from the website [36], a representation of all of the hydrofoils used was made in appendix A, where its possible to visualise the profile along with the generated 3D geometry in *SOLIWORKS*. For this study a dimension of 1000 millimeters was chosen for the chord length.

Chapter 3

Results And Discussion

3.1 2D CFD Validation

In order to be able to present the results with as much accuracy as possible, a previous simulation validation had to be done. For this we used a study from the National Advisory Committee of Aeronautics (NACA) themselves [34], and to better apply this study to our scenario only the angles of attack that fell into our spectrum were analysed, and done so according directly with the experimental testing for maximization of the accuracy. For this case the researchers analysed the profile through air so the term airfoil will be used for the validation scenario. The following test conditions are enumerated next:

- Airfoil dimensions:
    1. Chord = 1 meter
    2. Span = 1 meter
- Flow velocity = 20.73 [m/s] (Mach=0.060)
- Reynolds number per chord $\approx$ 1,419,149
- AoA = [0º, 2º, 4º,6º,8º]

Throughout this study several airfoil profiles were studied, the NACA 0012, from appendix A, was chosen in this case with the boundaries being in a C-shape formation where the inlet and side walls were 20 chord lengths from the airfoil, and the outlet 50 chord lengths after the airfoil. The following images categorize the boundary contions:

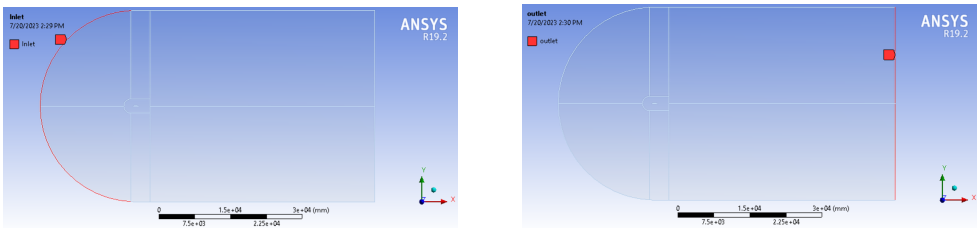

Figure 3.1: Full geometry with inlet and outlet highlighted, respectively.

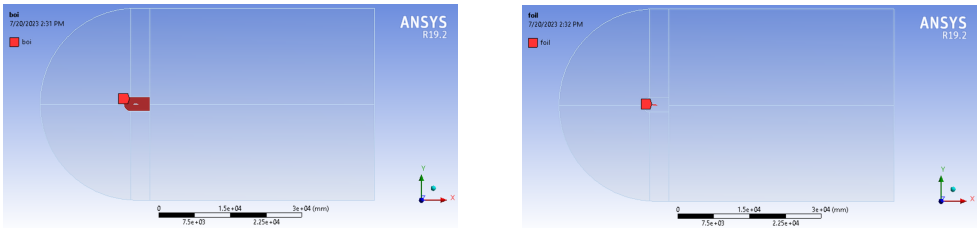

Figure 3.2: Full geometry with the body of influence (BoI) and foil highlighted, respectively.

For the meshing of the situation, tools such as edge and face sizing, meshing methods and inflation were used resulting in a total of around 183 000 nodes and elements, this later resulted in the best compromise between computacional time and accuracy.

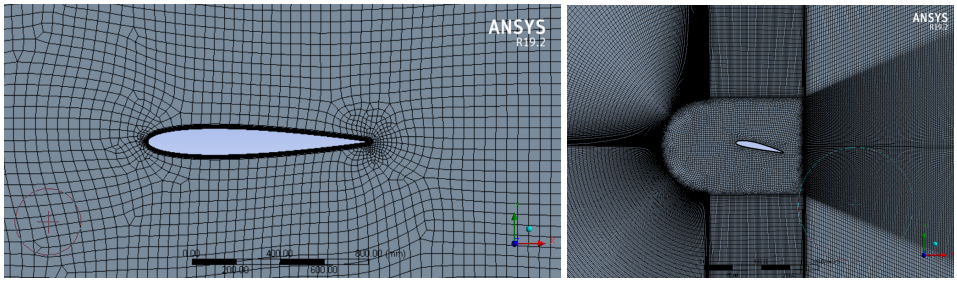

Figure 3.3: Generated mesh overview with the BoI and foil highlighted.

Since water can be assumed as an incompressible flow unlike air, a pressure-based solver was essential for the validation with air. This was a necessity so when it came to simulate with water the variation in density wouldn't cause accuracy loss. Furthermore, the time component was assumed steady given that there was only the need to evaluate the steady component of the calculations. Nevertheless, a comparison between the two was made with no apparent differences in simulation results.

An array of turbulence models were available however the most popularly used in the literature were the following:

- Spalart-Allmaras, Vorticity-Based (1 eqn)
- k-omega, Shear-Stress Transport (2 eqn)
- k-epsilon, Standard (2 eqn)

The decision between which to choose from became clear after the k-omega SST proved to demonstrate better results overall for the particular case of an AoA of 2º in table 3.1. A full numerical description of the governing equations and turbulence model was made in appendix D. Once the turbulence model was chosen we proceeded to complete the validation of the 2D simulations on the NACA 0012 airfoil, table 3.2 displays the obtained results.

Table 3.1: Performance comparison between some of the most used turbulence models in CFD

		Spalart-Allmaras	k-omega SST	k-epsilon Std
	AoA [º]	2	2	2
CFD	C_L [-]	0.2415	0.2403	0.2458
	C_D [-]	0.0099	0.0098	0.0105
	C_L/C_D [-]	24.369	24.509	23.465
EFD	C_L [-]	0.2213	0.2213	0.2213
	C_D[-]	0.0081	0.0081	0.0081
	C_L/C_D [-]	27.187	27.187	27.187
Error	C_L [%]	9.1279	8.6037	11.0709
	C_D [%]	21.745	20.467	28.686
	C_L/C_D [%]	10.363	9.848	13.688
Turbulent Inensity [%]		-	5	5
Turbulent Visc ratio [%]		10	10	10

Table 3.2: 2D validation results of the NACA 0012 airfoil

#Elements	183000		Flow Vel. [m/s]	20.730		
#Nodes	183000		Mach	0.060		

	AoA [º]	0	2	4	6	8
CFD	C_L [-]	0.0011	0.2142	0.4257	0.6450	0.8264
	C_D [-]	0.0117	0.0117	0.0131	0.0135	0.0183
	C_L/C_D [-]	0.0910	18.308	32.496	47.670	45.183
EFD	C_L [-]	0.0000	0.2000	0.4000	0.6000	0.8000
	C_D [-]	0.0090	0.0095	0.0098	0.0100	0.0130
	C_L/C_D [-]	0.0000	21.053	40.816	60.000	61.539
Error	C_L [%]	-	7.10	6.43	7.50	3.30
	C_D [%]	30.0	23.2	33.7	35.3	40.7
	C_L/C_D[%]	-	13.0	20.4	20.6	26.6

Chord [m]	1	$\tilde{C}_{L,Error}$ [%]	6.08
Span [m]	1	$\tilde{C}_{D,Error}$ [%]	32.6
Area [m^2]	1	$C_L\tilde{/}C_{D,Error}$ [%]	20.1

Most validation studies found in the literature focused only on the lift component, since the added drag by the profile tends to be some orders of magnitude smaller, this in turn means that, after convergence, for a close-to-fixed value fluctuation it tends be much harder to achieve a good simulation accuracy if the drag component is considered. By only taking the lift aspect into account we would have an accuracy close to 95%, whereas if we also include the drag component we could predict the results with around 81% accuracy, which is still a successful result. A comparison was also made between the relation of the number of elements with the CFD error in the next figure 3.4, and in figure 3.5 we have a graphical comparison between the obtained CFD results and the EFD values.

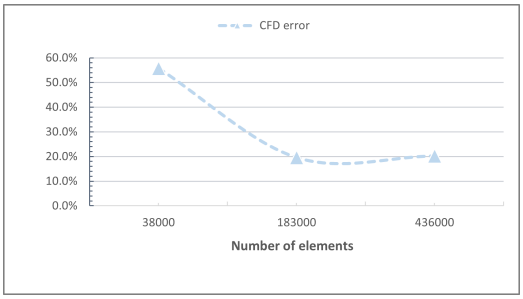

Figure 3.4: The computational error associated with the number of elements of the mesh.

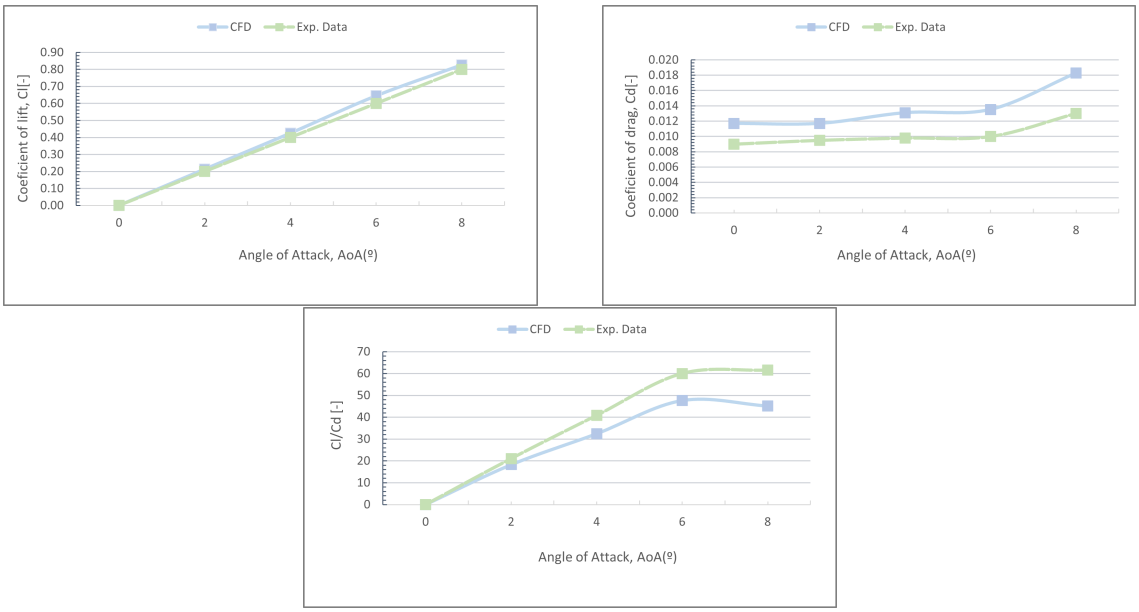

Figure 3.5: Evolution of the obtained CFD results as well as the EFD values of the coefficient of lift, coefficient of drag and the ratio between the two, respectively.

3.2 Hydrofoil Comparison

As it was mentioned previously there is an enumerous number of hydrofoils to choose from, since there was a time constraint present, only the hydrofoils with proven results were taken into account with the exception of two, in order to introduce some variety to the selected profiles.

Once the validation study was completed a thorough comparison between the eligible profiles could take place. We analysed for the angles of attack found in the literature as well as for an array of Froude numbers, limited only by the maximum speed of the Silent 120, of about 12 knots (6.174 m/s). Fortunately, these values fell amongst the ideal conditions for the application of a stern foil.

In the next figures the NACA 6418 profile is presented since it thrived under these testing conditions. The obtained CFD results, drag and lift values, velocity and pressure contours and residuals evolution, for the best scenario of 4º of AoA, are presented in the following table 3.3 and figures 3.6, 3.7 and 3.8.

Table 3.3: CFD results of the best hydrofoil profile, the NACA 6418

NACA 6418		Chord Length [m]	1		
		Vessel Length [m]	36.58	g[m/s^2]	9.81

Froude number	0.140	AoA [º]	2	**4**	6	8
Flow Vel. [m/s]	2.658	C_L[N]	3063.04	3780.40	4345.40	4521.92
Flow Vel. [knots]	5.166	C_D[N]	59.82	70.24	86.82	113.35
		C_L/C_D	51.20	53.82	50.05	39.89

Froude number	0.211	AoA[º]	2	**4**	6	8
Flow Vel. [m/s]	3.988	C_L[N]	6993.20	8646.54	10048.75	10460.06
Flow Vel. [knots]	7.751	C_D[N]	127.09	150.14	184.40	242.02
		C_L/C_D	55.03	57.59	54.49	43.22

Froude number	0.281	AoA[º]	2	**4**	6	8
Flow Vel. [m/s]	5.315	C_L[N]	12541.64	15524.17	18079.76	18920.44
Flow Vel. [knots]	10.332	C_D[N]	217.40	257.72	316.43	414.42
		C_L/C_D	57.69	60.24	57.14	45.66

Froude number	0.326	AoA[º]	2	**4**	6	8
Flow Vel. [m/s]	6.174	C_L [N]	16986.87	21040.55	24520.98	25786.03
Flow Vel. [knots]	12.000	C_D[N]	287.33	341.97	418.46	551.12
		C_L/C_D	59.12	61.53	58.60	46.79

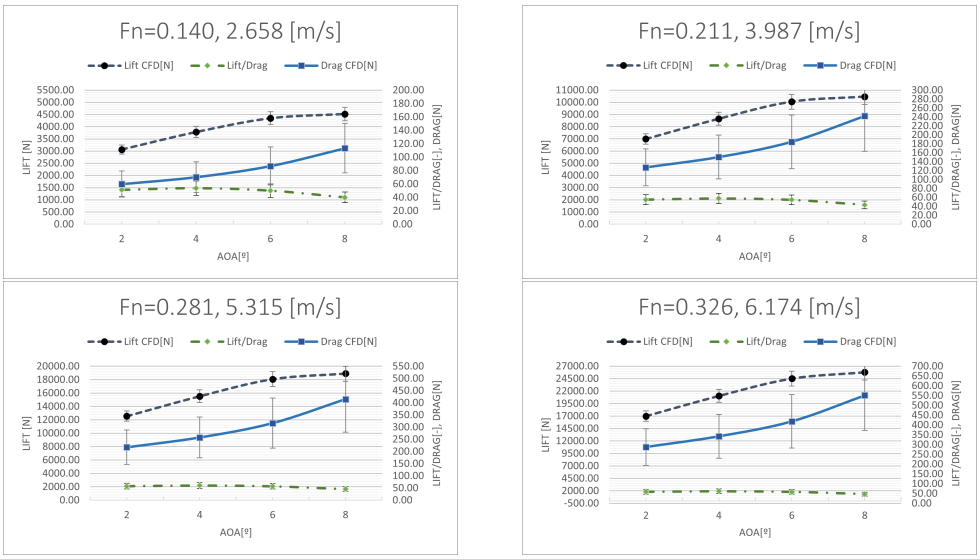

Figure 3.6: Evolution plot of the lift and drag forces for the different Froude numbers with the respective error variation.

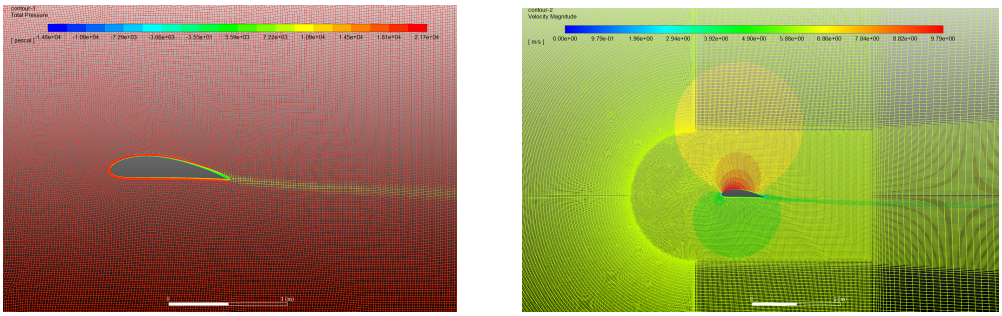

Figure 3.7: Obtained contours for the velocity magnitude and total pressure.

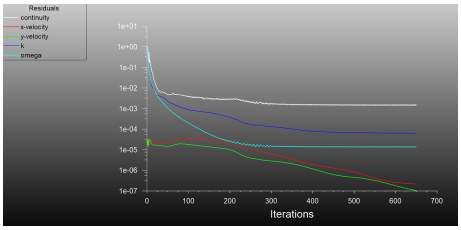

Figure 3.8: Residuals evolution from the best profile, the NACA 6418.

3.3 Ideal Positioning Of The Stern Foil

For this section, a 2D simulation was also performed in order to study the ideal positioning of the stern foil; since the best positioning of the stern foil was unknown we refrained from testing in a 3D scenario as it would only take more computational time and resorces. As you can imagine the combination of the vessel and hydrofoil was tested without struts. This was a necessary simplification in order to avoid an inaccurate 2D representation, and since the influence of the struts in the hydrodynamic performance can be neglected, this was the most logical step to take.

We initially included a parameter called "Dynamic Meshing". As we know the vessel would be experiencing a lift force from the stern caused by the hydrofoil, which would be slightly elevating the ship, for this behavior to be accurately represented software wise, we had to enable this feature to activate the degrees of freedom. In order to use the dynamic meshing feature a meshing technique called "Overset Meshing" had to be implemented, this allowed for 2 or more geometry profiles to merge in the fluent solver, after each one had gone through the meshing process. This parameter was essential for generating meshes with diferent levels of complexity and distinguishing between the geometry which would have degrees of freedom and the one which would maintain its position, or, in other words the background.

In order for the dynamic meshing to work it was required to input the following values from the table 3.4, regarding the dynamic properties of the vessel.

Table 3.4: Input values for *Ansys* of the hull properties of the Silent Yacht 120 such as mass and stress tensors, respectively

SY120 Hull Properties	
Mass [kg]	260000
I_{XX} [kg.m ^{2}]	1221000
I_{YY} [kg.m^2]	2452000
I_{ZZ} [kg.m^2]	3662000

Since the dynamic meshing feature allowed for degrees of freedom the computational domain was now in constant change; with the remeshing of the overset mesh, happening with each time-step, a far smaller time-step had to be chosen. This was a necessity since negative cell volumes would be created, and in turn simulation failure, if the changes in the domain were too great for the computational solver to follow. This implicitly meant a tenfold increase in the computational time.

This feature however proved ineffective at achieving realistic values. During the simulations we experienced a big fluctuation in the lift force, either the lift was close to the weight of the vessel, which was the ideal scenario, or it had high negative values. This behaviour could then be explained by the 2D profile of the ship which had an inverted bow, figure 3.9, this meant the negative lift generated by the upwards redirected flow of the inverted bow was in constant "battle" with the lift generated by the displaced volume of the vessel.

In order to solve this set-back the dynamic meshing feature was abandoned; with the vessel now in a fixed position we would inevitably obtain an elevated negative lift from the hull itelf. To be able to determine the best configuration, the set-up which would reduce the negative lift the most, would be the most ideal, since it would be the one where the most positive lift was added with the hydrofoil.

It's important to note that the lift force acting on the hull was chosen as the evaluation factor instead of the drag force, because the configuration with the highest lift would then have a greater impact on the trim correction and in turn a much greater reduction on the drag of the vessel. Since in this simulation set-up we are limiting the movement of the vessel, so no trim correction is allowed, the drag will be similar on all of the possible configurations since the wetted area will be the same.

For the simulation domain the objective is always to find the perfect balance between the ideal size, to minimize wall interferences, and computational time. Usually, for simulations such as this, the length of the object being tested is used as length dimension. The distance for wall-flow was designed to disallow disturbance flow near the model, it is intended that the calculation of ship resistance is not affected by waves caused from outside the model. The main dimensions in the

simulation were as follows: The inlet boundary, located at around 1-HL upstream from the bow of the ship (where HL is the hull's length at the water line), was defined as the inlet for fluid that equalled the ship's velocity; The outlet boundary, located at approximately 2-HL downstream from the transom of the ship, was also defined as the inlet boundary but at a constant pressure, which allowed incompressible flow in the scheme. Moreover, the bottom and top walls were located at 1-HL from the keel and 0.25-HL from the deck, respectively. In addition, the side wall was located at 1-HL from the longitudinal axis. The dimensions of the simulation are determined based on the practical guidelines of the International Towing Tank Conference, [35].

In the next images you can find a visual representation of the geometry used, figure 3.9, as well as the generated meshing component, figure 3.10; here it's possible to visualize the overset including the 2D hull and the enclosure which contains 2 bodies of influence, progressively increasing in size, along with a third BoI representing the waterline.

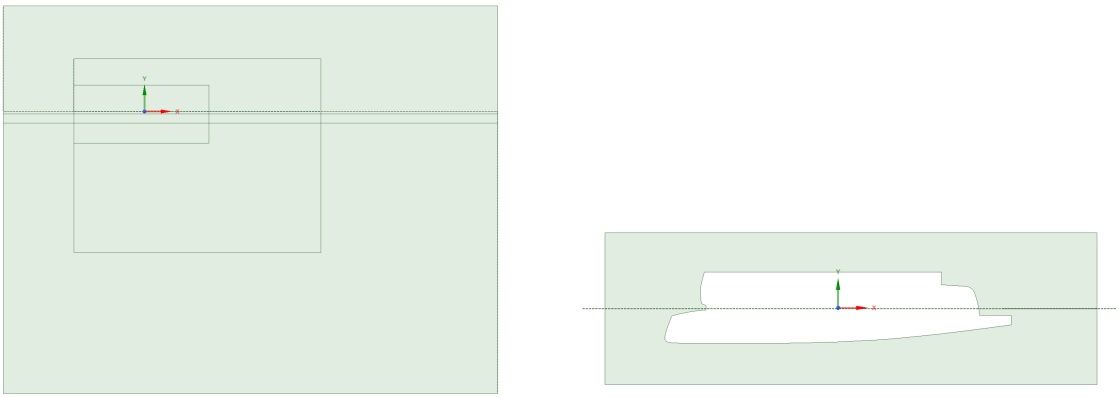

Figure 3.9: 2D geometry of the enclosure and overset, respectively.

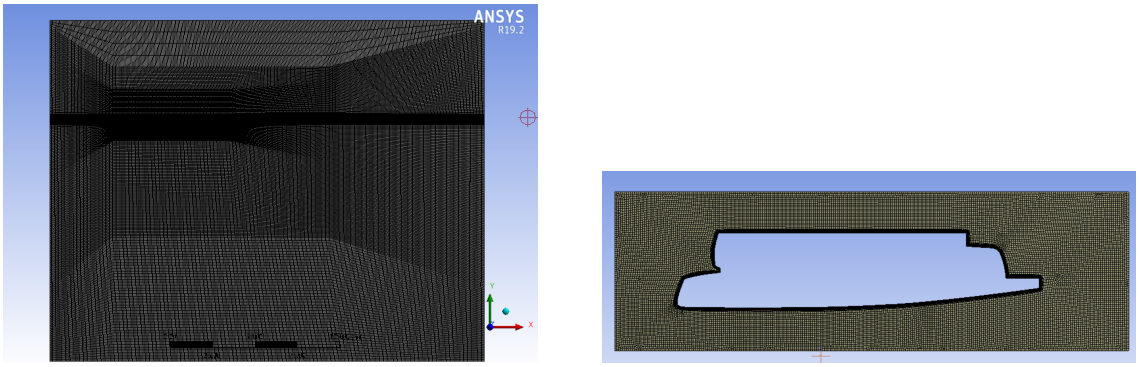

Figure 3.10: 2D mesh of the enclosure and overset, respectively.

In the next table, 3.5, we have an enumeration of the 5 tested positions along with their respective location regarding the stern and waterline. These 5 positions were chosen in order to understand the differences between an integrated stern foil and an appended stern foil, and for the

appended case the focus was to compreend the effect the distance from the stern/waterline had on the performance of the hydrofoil.

Table 3.5: Categorization of the location of the tested positions

Positioning	Distance From Stern [m]			
Distance From Waterline [m]	-0.5	0.5	1.0	1.5
0.60	-	Position 1	-	Position 3
0.85	-	-	Position 4	-
1.10	Position 5	Position 2	-	-

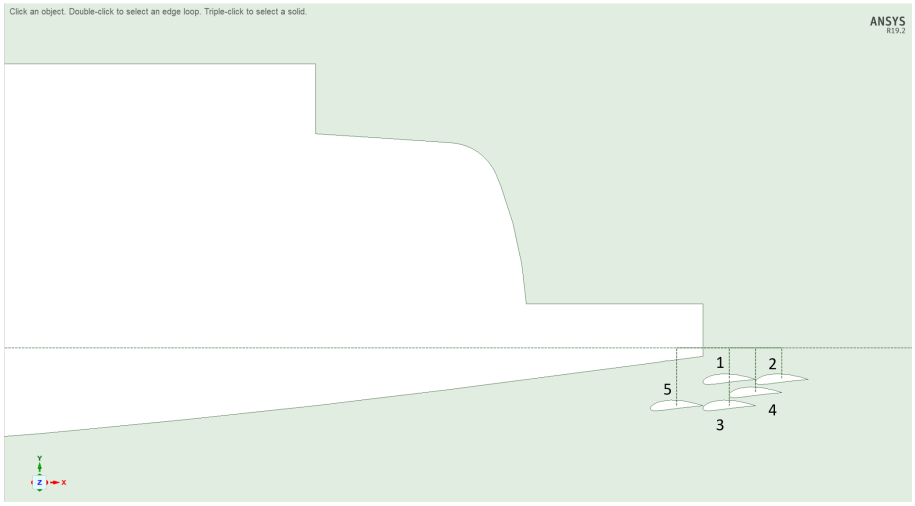

Figure 3.11: 2D geometry of the tested positions

3.3.1 2D Vessel With Stern Foil

Every simulation was done with the same ammount of time-steps, flow velocity and configuration set-ups in order to obtain the best possible comparison between all of the different scenarios. The simulation conditions were similar to the previous 2D hydrofoil comparison but with the following exceptions:

- Volume Of Fluid (VoF) configuration
- Constant flow velocity = 6,174 m/s
- Transient Solver
- Time-step = 0.05s
- Around 4000 time-steps
- About 200 seconds of flow analysis

As the flow increases in speed we can only see a very slight wake increase between the ship with no stern foil at 0 m/s, fig.3.12, and the ship with no stern foil at 6.174 m/s, fig.3.13. This serves as a reminder of the fixed set-up used, which neglects any occurring sinkage of the vessel at higher speeds, and in turn automatically reduces the generated wake. This comes to show that even in a scenario where the generated wake is already in a reduced state, the stern foil can diminish the wave generation in a considerable manner. The following table 3.6 shows the 2D simulation results of the overall lift force.

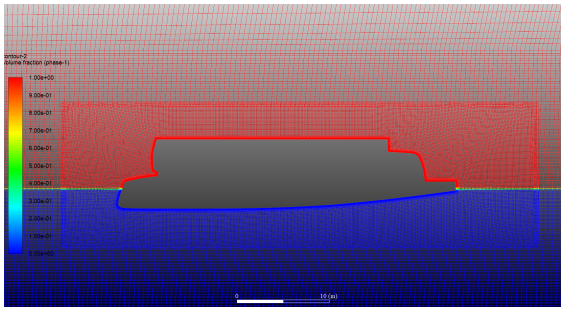

Figure 3.12: 2D phase representation of the ship in its initial state at 0 m/s.

Table 3.6: Lift force results from the 2D simulations of the 5 possible positions

Positions	Lift force [N]	Lift increase [N]
Baseline	-1089730.20	-
Position 1	-1076736.60	12993.60
Position 2	-1080638.80	9091.40
Position 3	-1084258.70	5471.50
Position 4	-1077884.10	11846.10
Position 5	-1085251.80	4478.40

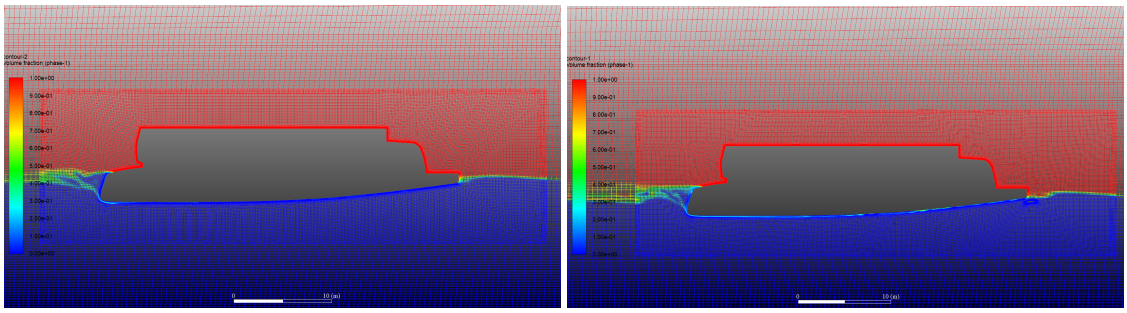

Figure 3.13: 2D phase representation of the ship baseline values and the ship with the stern foil in its best position, postion 1, at 6.174 m/s, respectively.

The images above display the comparison between best positioning, out of the ones tested, and the baseline configuration, fig.3.13. Here we have a clear visual representation of the reduction

in the generated wake behind the transom of the vessel; this reduction which originated from the lift force created by the stern foil, was no more than the effects of the low pressure zone of the hydrofoil on the passing flow.

The complete representation of the results can be found in Appendix C. Its noteworthy that several other positions could have been chosen and evaluated.

It is important to mention that the results represent in no way shape or form, accurate results from a realistic point of view, since the 2D representation of the vessel was also not ideal. The single purpose of this analysis was to understand under these conditions, where all of the hydrofoil positions were being evaluated in the same testing circumstances, which would be the most ideal.

All of these configurations would be beneficial to the vessel since all performed very similarly. Nevertheless, we can now confirm that the integrated stern foil, position 5, performed the worst, a result which was also seen from the HV developers, [20], and as you increase in depth, as well as the distance from the stern the performance of the hydrofoil gradually decreases, conclusion which was also seen by [9].

To conclude this section the position which performed the best was position 1, however this was not the ideal scenario for Silent Yachts since this would imply an increase in overall vessel length and thoughts would now have to be given towards passenger safety and docking maneuvers. If the position 1 configuration presented too many challenges, the position 5 configuration would take place instead. In any case, the set-up of position 1 will be used to achieve the best possible results.

3.4 3D Silent Yacht With Stern Foil

Once the best positioning was chosen it was time for the 3D simulations. One with only the hull itself and the other with the stern foil. Here once again we employed the same ideology used before for the 2D simulations with the vessel, however, in this case the dynamic meshing feature could work as intended. For this scenario the Silent 120 only had the freedom to move in the vertical axis; with a vessel of this size sailing at slow speeds in ideal conditions, the visible pitch would already be minimal, and because we would be working with an extremely large fluid domain, the decision to limit rotation and the remaining degrees of freedom, was made to simplify the simulation conditions and shorten the computational time. This, obviously, would imply a small decrease in the accuracy of the simulation results.

In order to reduce computational cost, the distance between the vessel and the walls was shortened, but with very similar proportions to the previous 2D scenario of the vessel, as it can be seen in the following figures 3.14 and 3.15. Now with the simulation domain considerably larger having the right meshing of the geometry is one of the most important components, if not the most

important, in order obtain an accurate solution within a reasonable computational effort. For this simulation there was always a constant search for a balance between the number of elements in the meshing and the ideal time-step to achieve optimum convergence.

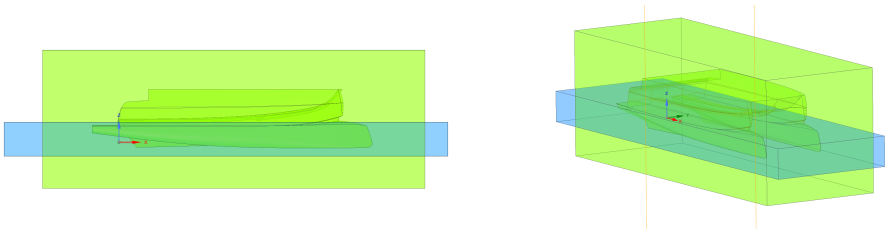

Figure 3.14: 3D representation of the overset and a BoI for the waterline

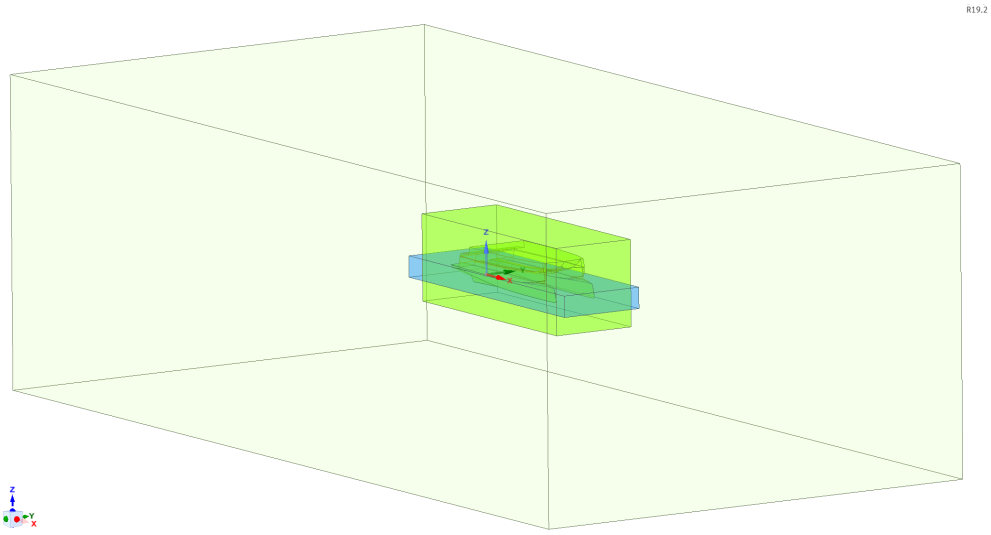

Figure 3.15: 3D representation of the enclosure overlapping the overset and waterline

It's important to note that we took advantage of the symmetry of the vessel; now with the xz symmetry plane we could divide the fluid domain in half, which would allow for more element density and, most importantly, more computational speed. With a concern to achieve the most accurate results possible we decided to have a relative high number of nodes and elements, both for the overset and enclosure. with the overset and enclosure meshing having above 800 000 nodes and 800 000 elements. As you can see the element density in the overset is far superior to the enclosure, since most fluid interactions will happen within the overset.

Some of the techniques used in the meshing process were: inflation to cover the boundary layer, edge subdivision with bias towards the vessel, to progressively increase the element density as we moved closer to the vessel, and a BoI to again increase the element density in the specified area of the waterline.

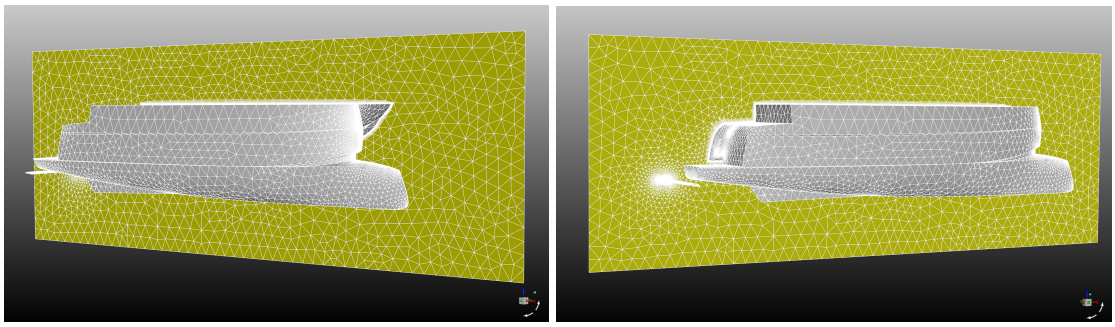

Figure 3.16: 3D representation of the hull and symmetry plane on the overset mesh

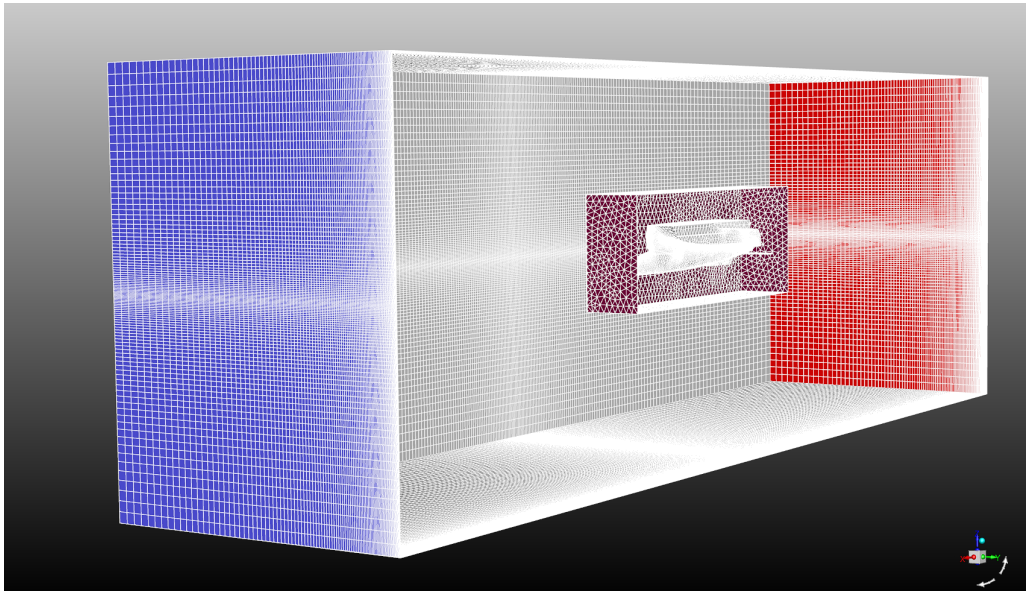

Figure 3.17: 3D representation of the enclosure mesh with inlet, farfield, outlet and overset.

From the upcoming table 3.7 we can see the progressive increase in the number of elements in order to obtain simulation convergence, which, unfortunantely, wasn't achieved. Even with all of the previous methodologies to reduce computational effort, the processing power demanded was just too great for the computer used throughout this thesis. As the simulation increased in complexity the computational time also increased but in an exponential manner; from two to three hours in the first simulations to complete days in the last, as we continued our efforts it became harder and harder to perform either variations to the meshing or simulation configurations.

Table 3.7: 3D Simulation conditions tested

Set-up #	Overset #Elements	Enclosure #Elements	Time-step	Convergence
1	500 000	250 000	0.010	Failed
			0.005	
			0.001	
2	600 000	350 000	0.010	Failed
			0.005	
			0.001	
3	600 000	700 000	0.010	Failed
			0.005	
			0.001	
4	850 000	800 000	0.010	Failed
			0.005	
			0.001	
5	2 100 000	1 800 000	0.010	Failed
			0.005	
			0.001	

In the end, the outcome of all of the simulations was the same, as the vessel started to move vertically, the position variations weren't being correctly transfered through the elements in the meshing, so the k residuals, responsible for the turbulence model, would start to gradually increase, and, eventually, would reach such values that this increase would cascade into the continuity residuals which are, in simple terms, the defining factor for convergence. These small variations would turn a reasonably stable simulation into a floating point exception error, in a matter of just a few iterations. In figures 3.18 to 3.19 it's possible to visualize this evolution.

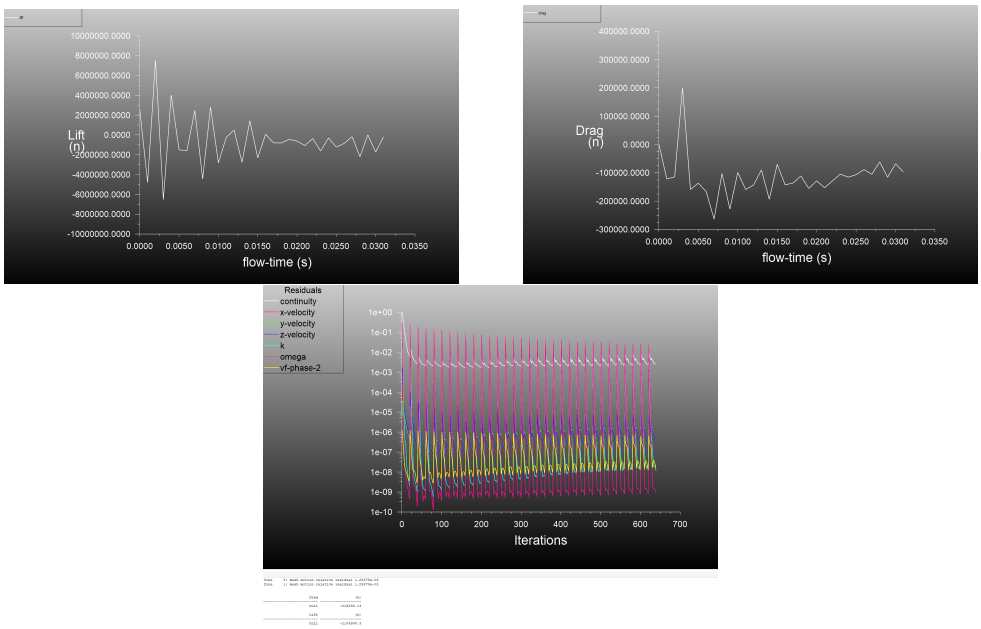

Figure 3.18: 3D simulation results from the last simulation before floating point exception error

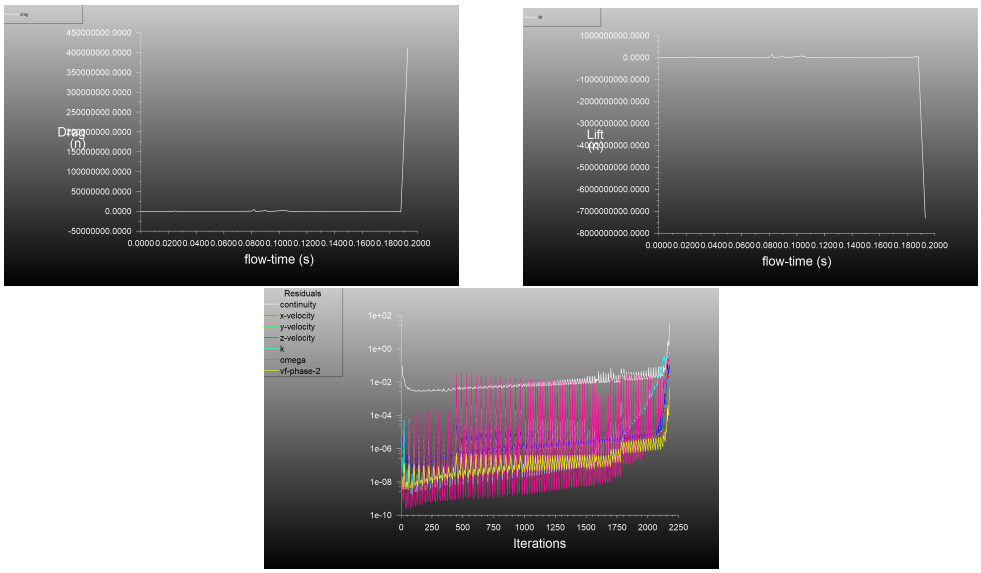

Figure 3.19: 3D simulation results from the last simulation after floating point exception error

Even though convergence was never achieved, it was possible to visualize a gradual increase in simulation stability. The obvious solution to the problem would be to continue to increase in element density, to more accurately control the changes occurring during the simulation. This would also implicitly mean a far greater computational effort would be demanded.

3.5 Discussion

Throughout this analysis countless different geometries were tested and simulated; from the 1 meter hydrofoil profiles to the 36.58 meter hull geometry, every step taken became progressively bigger and more challenging, all in the pursuit of a solution to reduce the hull resistance of the Silent Yacht 120.

Upon finding the ideal hydrofoil profile, the NACA 6418, we proceeded to discover where the best placement could be. Even though the ideal placement wouldn't have made that much of an impact on the performance of the hydrofoil, it was a procedure that proved useful to understand the performance behavior regarding the change in depth and distance from the stern. A tendency to reduce the performance of the stern foil was seen when both the distance from the waterline and stern increased.

Finally, with the stern foil profile conceived and fixed in position 1, the final 3D analysis was made but, unfortunantely, not completed. Here we would truly understand if the impact created by the stern foil would be positive or negative and in a quantifiable manner.

Given the very delicate power balance within the entire vessel, between the solar panels, the battery and the generator we thought it would be more interesting if we presented the results in terms of gained or lost energy flux.

As we know the power required for an object to overcome it's drag, for a desired fluid, is the drag force of the object times the relative flow velocity; therefore we determined the gain in energy for every time the vessel would cruise at the designed speed of 12 knots; through the equation 3.1 we would calculate the power required to sail at 12 knots (6 m/s) with and without the stern foil.

$$P = F_D * V[w] \tag{3.1}$$

Chapter 4

Conclusions And Future Work

4.1 Stern Foil or Not?

To conclude, its clear the stern foil benefits from a simple instalation with almost no maintenance required, and upon its installment a constant power reduction would be seen, for the designed speed, without any dependency on power sources or auxiliar systems.

It could even go as far as increasing the range of the vessel by such an amount that the battery size could be reduced, directly affecting the ship dynamics by reducing weight or by increasing space for other utilities and/or necessities.

Throughout this study countless different geometries were tested and analysed. From the 1m hydrofoils to the 36m hull, every step taken became progressively bigger and more challenging , all in the pursuit of a solution to reduce the hull resistance of the Silent 120. Even though we weren't able to achieve a final answer, we acquired the best geometry to use, the NACA 6418, and the best positioning, position 1, in order to obtain the best possible results regarding the this application of the stern foil.

In the end, the company greatly appreciated the work done during this thesis since it now gave them a clear perspective on the potential that a stern foil could bring to their vessels, and a foundation for further related studies. The only question that remained was if the placement of the stern foil would continue in position 1 or if position 5 could prove more benefitial, logistically.

4.2 Future Work And Recomendations

As it can be expected this thesis did not undergo all of the conceivable variables of a real life scenario. Understandably, due to complexity and a shortage of time, both in computing resources and

physical duration, this study only took on the major variables that influenced the total resistance reduction of the hull. These being:

1. Stern foil profile
2. Angle of attack
3. Stern foil positioning

If additional time was to be dedicated to this project the following topics should be evaluated:

- In order to study the validity for a real life scenario a towing tank test should be taken into account.
- Even though several hydrofoil profiles were studied there could exist a better suited profile, chord length or chord thickness for this particular scenario.
- In terms of technology, systems with variability on the angle of attack already exist and could prove extremely beneficial to avoid the additional drag outside the designed velocity.
- A situation with waves should be highly fascinating in terms of demonstrating both the seakeeping improvements, such as pith and heave, as well as the total resistance reduction from those seakeeping improvements.
- Modifications to the shape of the hydrofoil itself where cavitation improvements could take place, either with protuberances imitating the bolbus bow phenomena or with addition of vortex generators, amoung many other alternatives, should prove beneficial.
- Because the inter-hull flow isn't uniform in comparison with the flow on the hulls themselves, an alteration to the positioning/AOA of the section of stern foil in between the two hulls might be advantageous. Since in catamarans the bridging flow tends to be slightly elevated, the stern foil should follow this wave height difference.
- Since *ANSYS* is such a complex software, I only grasped its potential for applications such as this, so additional time should be dedicated to the many useful tools yet to be exploited.
- This study only evaluated the effects of the stern foil for the maximum speed of the vessel, 6.174 m/s, in order to maximize its benefits. A comparison between the full range of speeds should prove extremely interesting to see if even at cruising speeds we would be able to have some drag reduction.

Finally, the ideal scenario would be to produce a prototype and with sea trials confirm or deny the CFD calculations. Even though this component has already proven its usability in monohulls the results could prove disheartening since this is, in it's entirety, a novel application in catamarans.

Appendix A

Hydrofoil Profiles

In this section are listed the hydrofoil profiles considered for this thesis. Where the images will include the individual characteristics of each one. All profiles came from the NACA database [36][1]. All of the profiles were imported into **SOLIDWORKS** to then again be imported into **ANSYS** for the hydrodynamic comparison.

The hydrofoils were generated with a closed trailing edge and with the maximum amount of points available which was 200.

[1] Available at http://airfoiltools.com/

A.1 Symmetrical Hydrofoils

A.1.1 NACA 0012

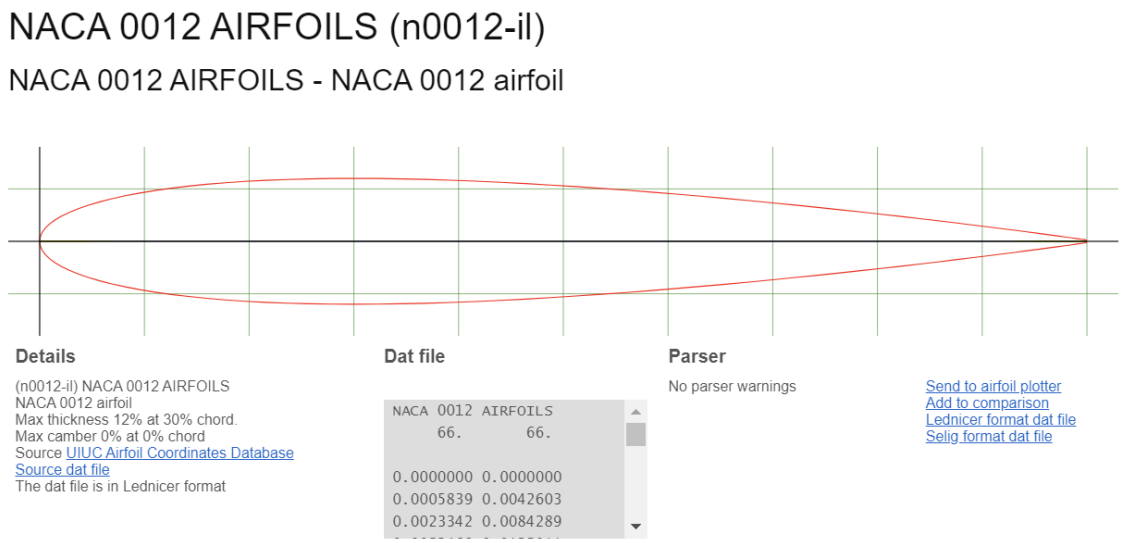

Figure A.1: NACA 0012, [7], [8].

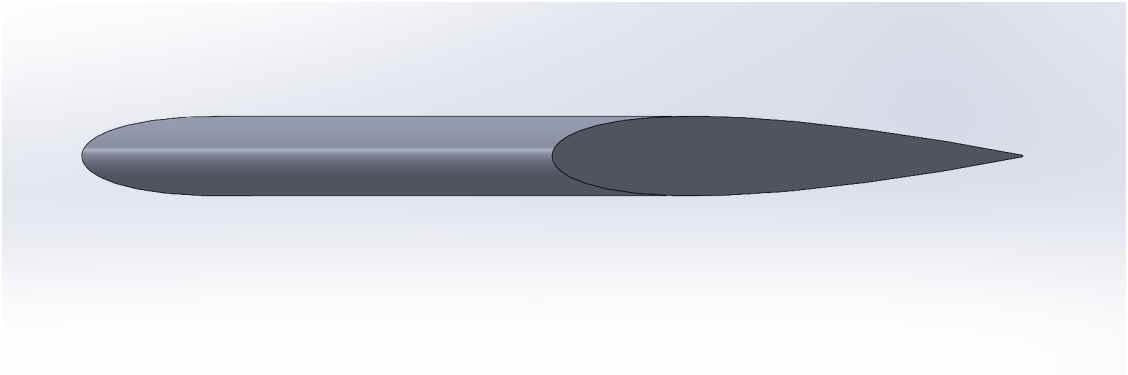

Figure A.2: NACA 0012 in *SOLIDWORKS*, [7], [8].

A.1.2 NACA 0018

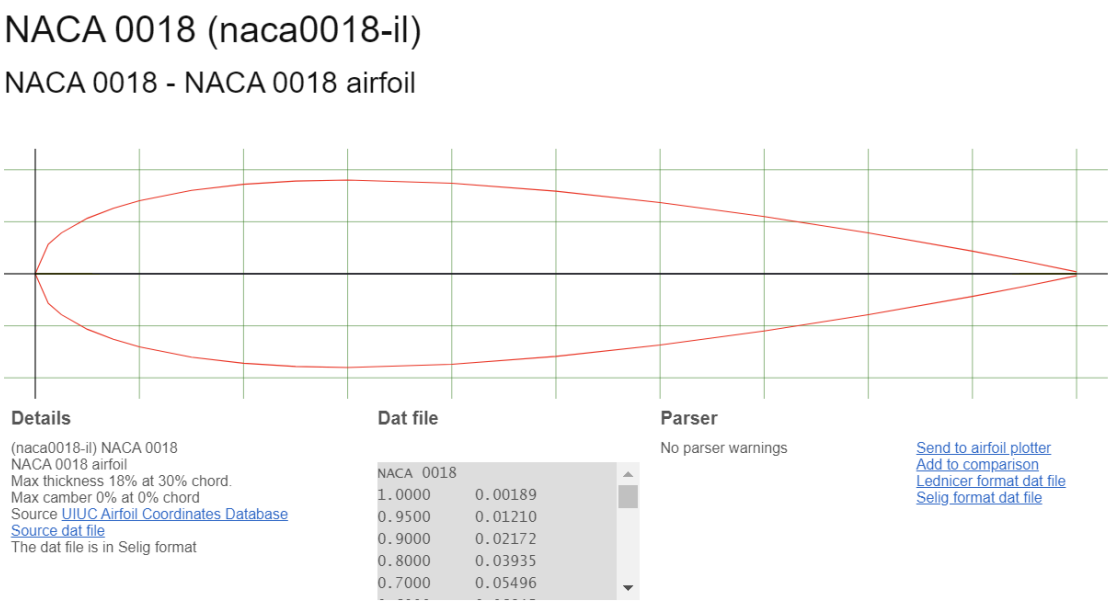

Figure A.3: NACA 0018, [8].

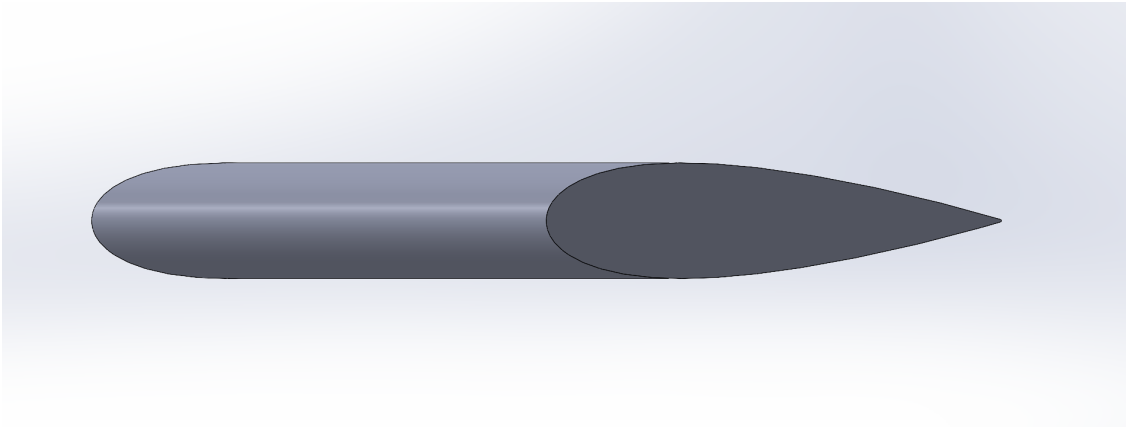

Figure A.4: NACA 0018 in *SOLIDWORKS*, [8].

A.2 Asymmetrical Hydrofoils

A.2.1 NACA 2412

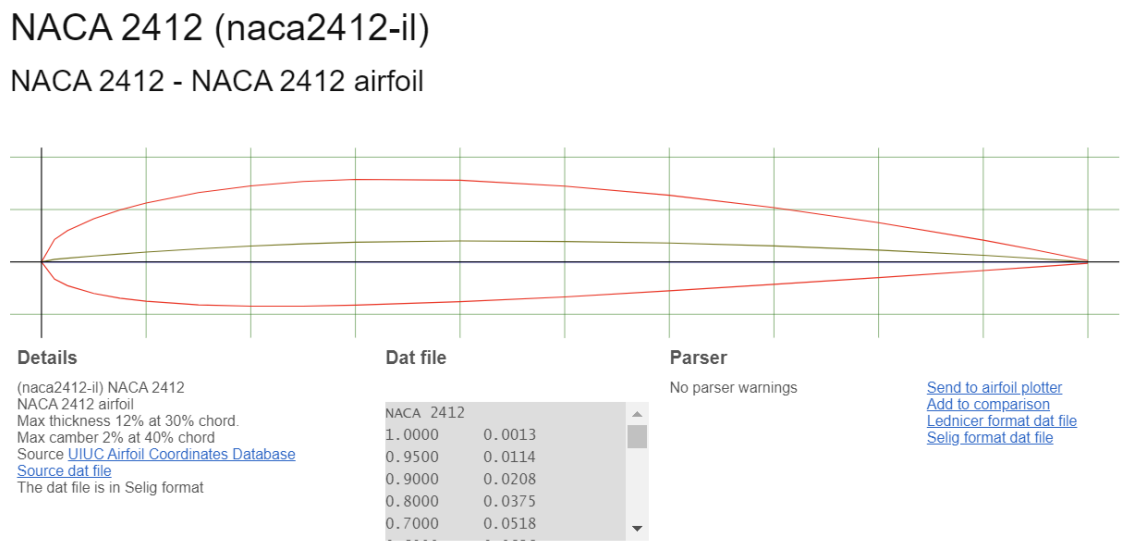

Figure A.5: NACA 2412, [8].

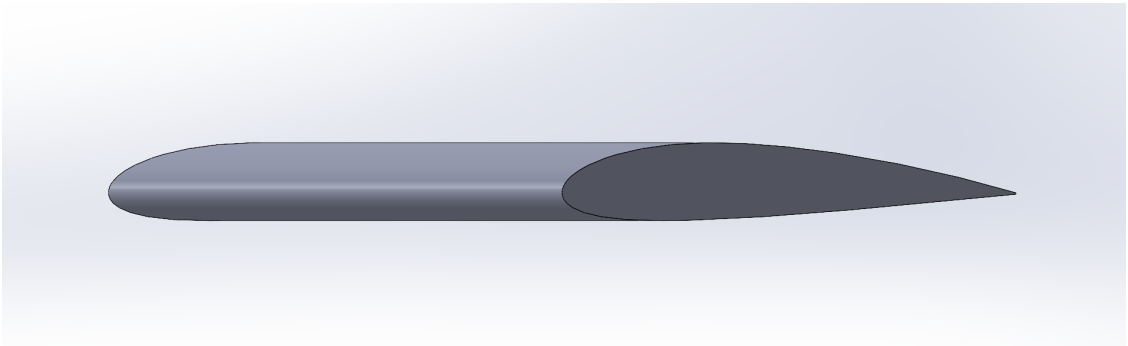

Figure A.6: NACA 2412 in *SOLIDWORKS*, [8].

A.2.2 NACA 4409

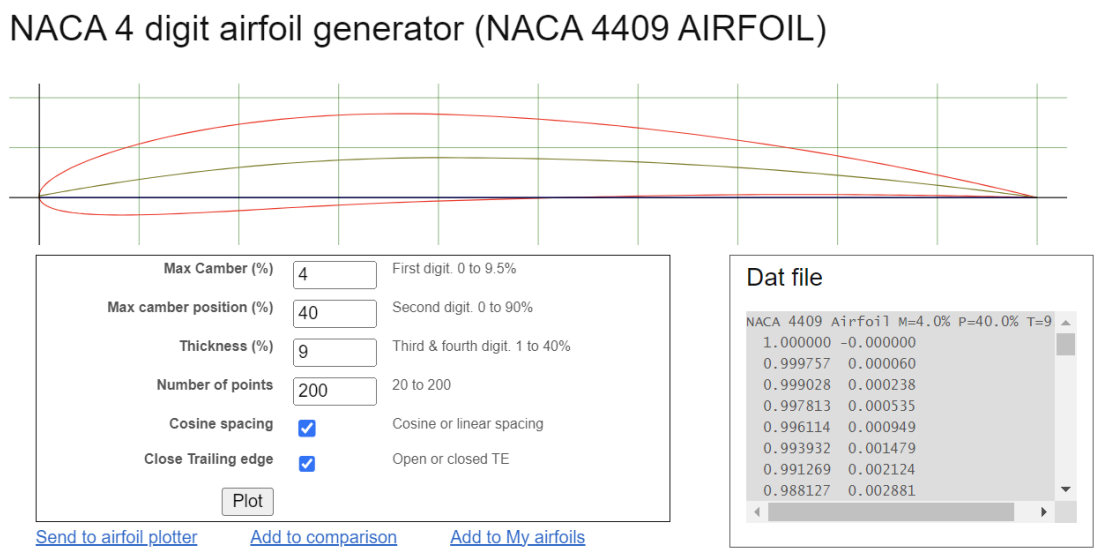

Figure A.7: NACA 4409.

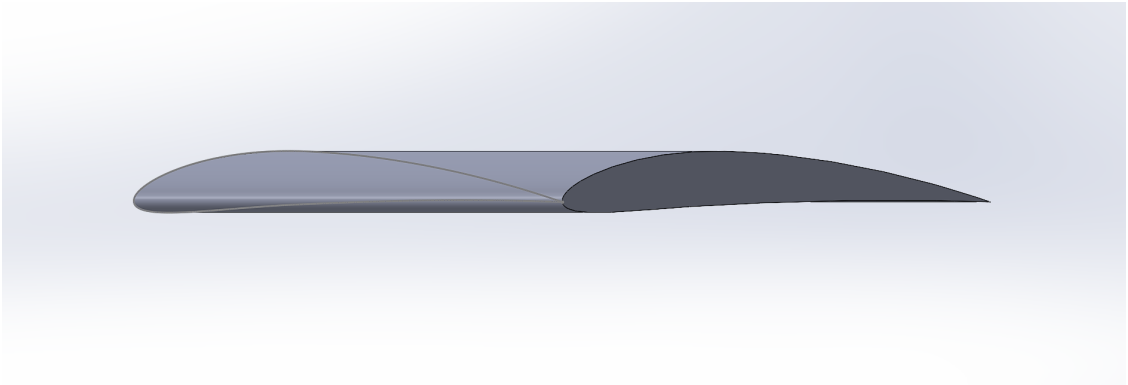

Figure A.8: NACA 4409 in *SOLIDWORKS*, [8].

A.2.3 NACA 4412

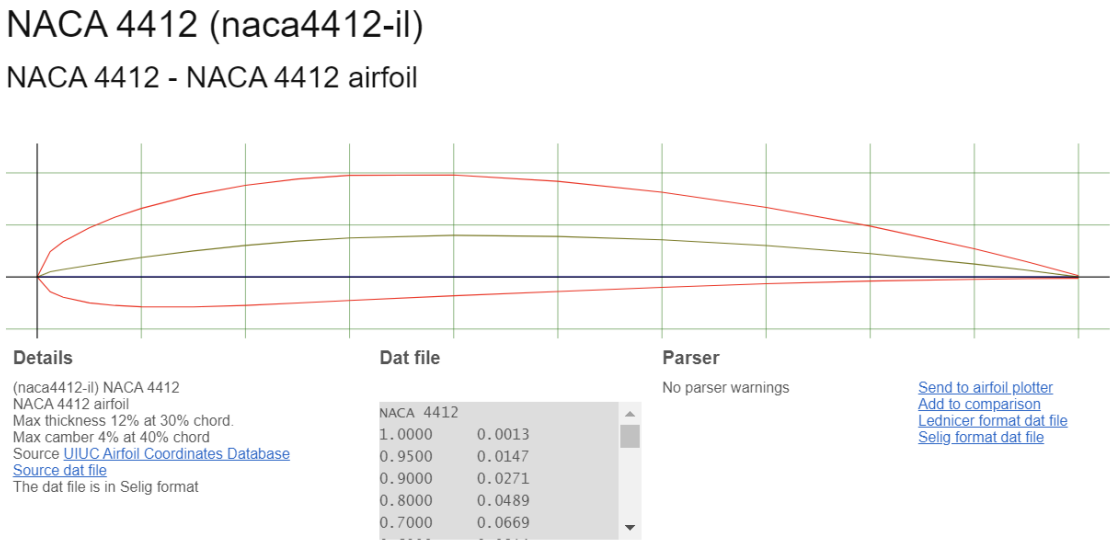

Figure A.9: NACA 4412, [9], [10], [11], [12], [13].

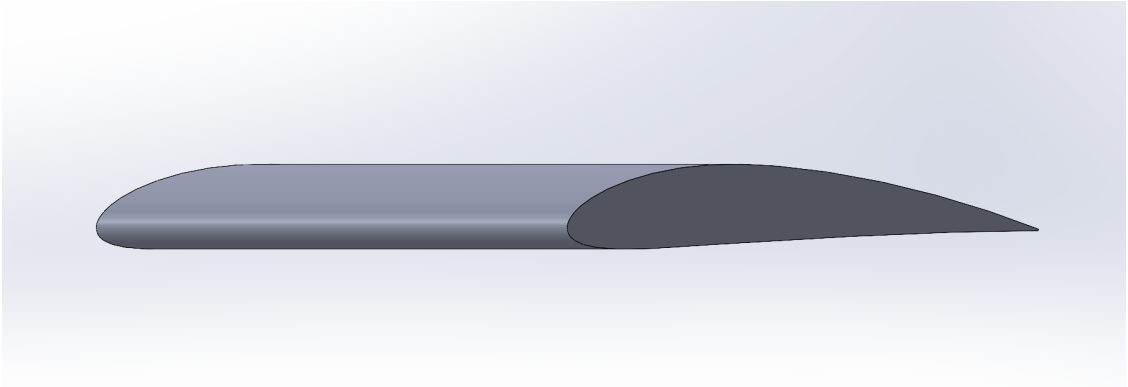

Figure A.10: NACA 4412 in *SOLIDWORKS*, [9], [10],[11], [12], [13].

A.2.4 NACA 4418

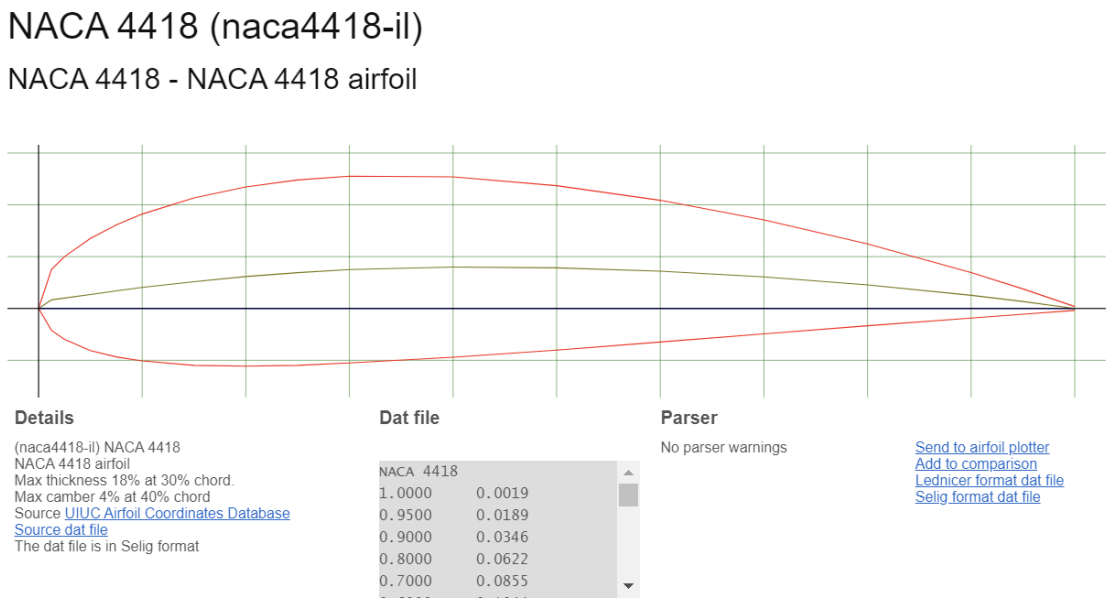

Figure A.11: NACA 4418, [14].

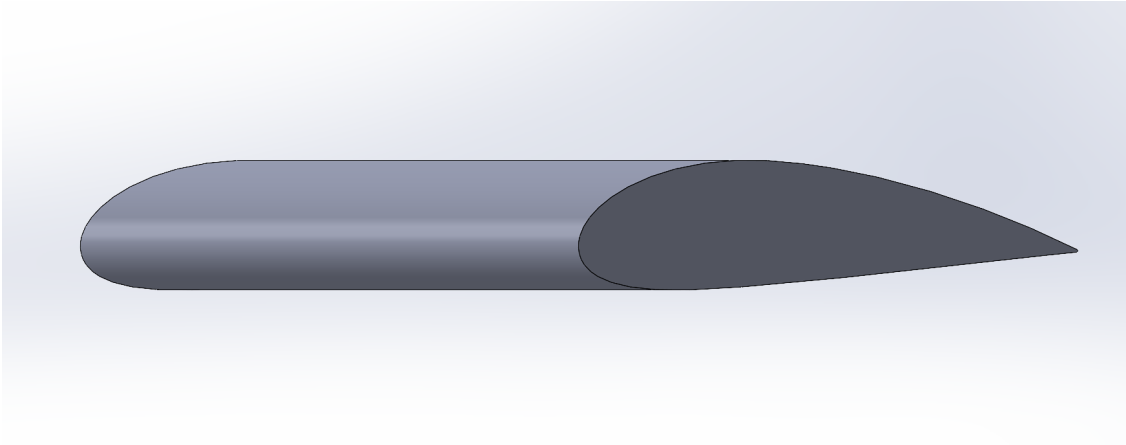

Figure A.12: NACA 4418 in *SOLIDWORKS*, [14].

A.2.5 NACA 6418

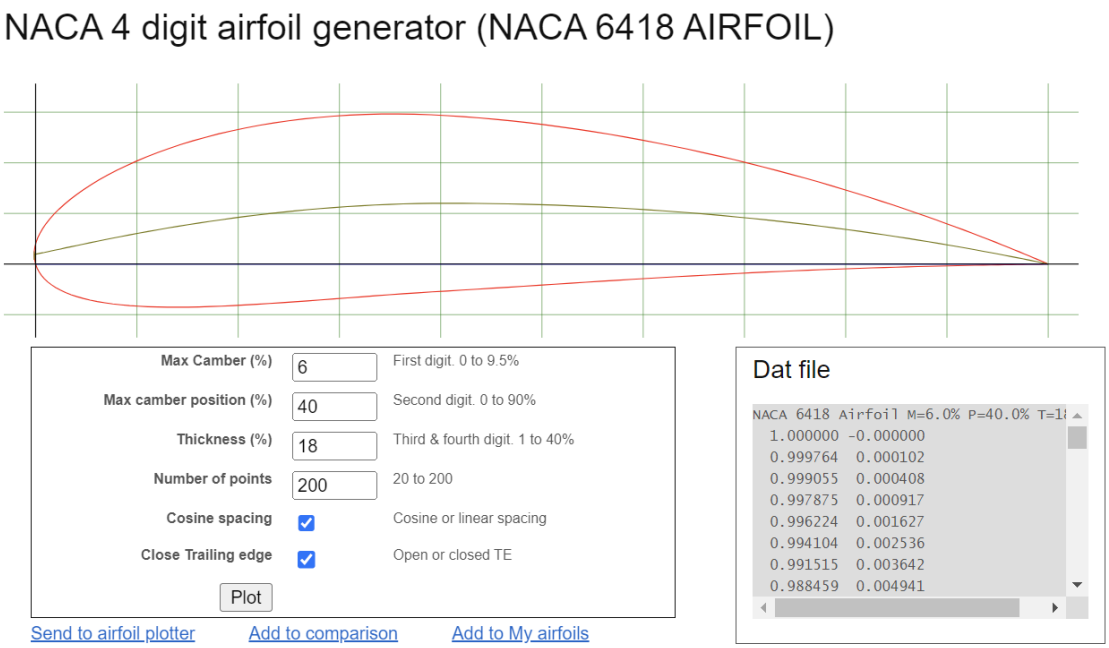

Figure A.13: NACA 6418.

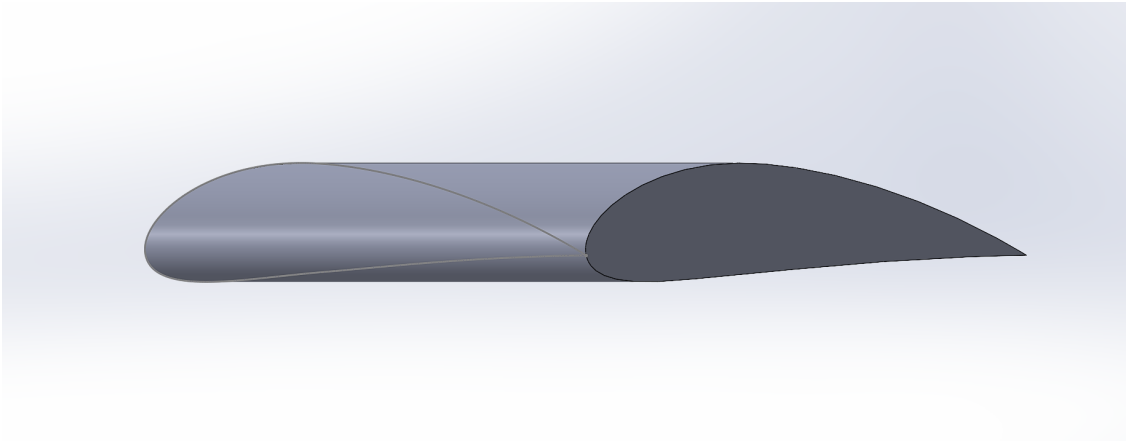

Figure A.14: NACA 6418 in *SOLIDWORKS*.

Appendix B

Computational Fluid Dynamics Results

In this appendix you will find all of results obtained from the CFD computations. Here there will be presented both the 2D simulations for the hydrofoils as well as the 2D for the vessel and hydrofoil. Along side these the final 3D simulation will also be included.

B.1 Hydrofoil Comparison

This comparison to determine the best hydrofoil out of the ones selected took place with the same geometry design, same number of elements and nodes and the same testing conditions:

- Aerofoil dimensions and testing conditions:
    1. Chord = 1 meter
    2. Span = 1 meter
- Flow: Air
- Flow velocity [m/s] = 2.658, 3.988, 5.315 and 6.174.
- AoA = [0º, 2º, 4º,6º,8º]

B.1.1 NACA 0012

Table B.1: CFD results of the NACA 0012 hydrofoil profile

NACA 0012		Chord Length[m]	1		
		Vessel Length[m]	36.58	g[m/s2]	9.81

Froud number	0.140	AoA[°]	2	4	6	8
Flow Vel. [m/s]	2.658	C_L[N]	758.03	1513.34	2245.51	2968.06
Flow Vel. [knots]	5.166	C_D[N]	37.34	41.57	49.01	58.92
		C_L/C_D	20.30	36.40	45.82	50.37

Froud number	0.211	AoA[°]	2	4	6	8
Flow Vel. [m/s]	3.988	C_L[N]	1719.31	3426.58	5086.22	6729.95
Flow Vel. [knots]	7.751	C_D[N]	79.36	88.73	105.25	127.18
		C_L/C_D	21.66	38.62	48.33	52.92

Froud number	0.281	AoA[°]	2	4	6	8
Flow Vel. [m/s]	5.315	C_L[N]	3066.57	6113.39	9079.55	12020.87
Flow Vel. [knots]	10.332	C_D[N]	135.99	152.49	181.53	219.96
		C_L/C_D	22.55	40.09	50.02	54.65

Froud number	0.326	AoA[°]	2	4	6	8
Flow Vel. [m/s]	6.174	C_L[N]	4144.37	8261.71	12281.56	16262.37
Flow Vel. [knots]	12.000	C_D[N]	180.01	202.11	241.29	292.66
		C_L/C_D	23.02	40.88	50.90	55.57

B.1.2 NACA 0018

Table B.2: CFD results of the NACA 0018 hydrofoil profile

NACA 0018		Chord Length[m]	1		
		Vessel Length[m]	36.58	g[m/s2]	9.81

Froud number	0.140	AoA[°]	2	4	6	8
Flow Vel. [m/s]	2.658	C_L[N]	727.31	1445.04	1962.81	2110.93
Flow Vel. [knots]	5.166	C_D[N]	54.23	65.28	84.74	126.32
		C_L/C_D	13.41	22.14	23.16	16.71

Froud number	0.211	AoA[°]	2	4	6	8
Flow Vel. [m/s]	3.988	C_L[N]	1653.42	3274.17	4471.62	4832.57
Flow Vel. [knots]	7.751	C_D[N]	116.92	142.04	185.27	276.82
		C_L/C_D	14.14	23.05	24.14	17.46

Froud number	0.281	AoA[°]	2	4	6	8
Flow Vel. [m/s]	5.315	C_L[N]	2950.96	5845.28	8011.59	8690.68
Flow Vel. [knots]	10.332	C_D[N]	201.70	246.02	323.30	484.31
		C_L/C_D	14.63	23.76	24.78	17.94

Froud number	0.326	AoA[°]	2	4	6	8
Flow Vel. [m/s]	6.174	C_L[N]	3995.32	7898.88	10850.01	11785.52
Flow Vel. [knots]	12.000	C_D[N]	268.03	327.26	431.79	647.47
		C_L/C_D	14.91	24.14	25.13	18.20

B.1.3 NACA 2412

Table B.3: CFD results of the NACA 2412 hydrofoil profile

NACA 2412		Chord Length[m]	1		
		Vessel Length[m]	36.58	g[m/s2]	9.81

Froud number	0.140	AoA[°]	2	4	6	8
Flow Vel. [m/s]	2.658	C_L[N]	1532.63	2229.02	2566.98	2748.06
Flow Vel. [knots]	5.166	C_D[N]	51.60	70.4	128.61	172.93
		C_L/C_D	29.70	31.66	19.96	15.89

Froud number	0.211	AoA[°]	2	4	6	8
Flow Vel. [m/s]	3.988	C_L[N]	3463.99	5038.071	5720.04	6235.91
Flow Vel. [knots]	7.751	C_D[N]	112.25	155.21	288.53	383.64
		C_L/C_D	30.86	32.46	19.82	16.25

Froud number	0.281	AoA[°]	2	4	6	8
Flow Vel. [m/s]	5.315	C_L[N]	6168.94	8971.28	10495.36	11152.04
Flow Vel. [knots]	10.332	C_D[N]	194.40	272.16	500.53	675.59
		C_L/C_D	31.73	32.96	20.97	16.51

Froud number	0.326	AoA[°]	2	4	6	8
Flow Vel. [m/s]	6.174	C_L[N]	8333.14	12119.29	13992.14	15064.11
Flow Vel. [knots]	12.000	C_D[N]	259.19	364.11	683.55	908.7307
		C_L/C_D	32.15	33.28	20.47	16.58

B.1.4 NACA 4409

Table B.4: CFD results of the NACA 4409 hydrofoil profile

NACA 4409		Chord Length[m]	1		
		Vessel Length[m]	36.58	g[m/s2]	9.81

Froud number	0.140	AoA[°]	2	4	6	8
Flow Vel. [m/s]	2.658	C_L[N]	1772.62	2579.23	2952.99	3189.71
Flow Vel. [knots]	5.166	C_D[N]	59.45	59.50	96.09	145.06
		C_L/C_D	29.82	43.35	30.73	21.99

Froud number	0.211	AoA[°]	2	4	6	8
Flow Vel. [m/s]	3.988	C_L[N]	3976.85	5788.70	6671.57	7186.85
Flow Vel. [knots]	7.751	C_D[N]	129.64	129.84	213.70	324.23
		C_L/C_D	30.68	44.58	31.22	22.17

Froud number	0.281	AoA[°]	2	4	6	8
Flow Vel. [m/s]	5.315	C_L[N]	7080.53	10303.92	11908.20	12820.74
Flow Vel. [knots]	10.332	C_D[N]	226.14	226.93	377.27	575.65
		C_L/C_D	31.31	45.41	31.56	22.27

Froud number	0.326	AoA[°]	2	4	6	8
Flow Vel. [m/s]	6.174	C_L[N]	9558.50	13914.26	16098.11	17329.48
Flow Vel. [knots]	12.000	C_D[N]	302.18	303.41	507.73	774.91
		C_L/C_D	31.63	45.86	31.71	22.36

B.1.5 NACA 4412

Table B.5: CFD results of the NACA 4412 hydrofoil profile

NACA 4412		Chord Length[m]	1		
		Vessel Length[m]	36.58	g[m/s2]	9.81

Froud number	0.140	AoA[°]	2	4	6	8
Flow Vel. [m/s]	2.658	C_L[N]	2318.81	3077.95	3538.87	3449.61
Flow Vel. [knots]	5.166	C_D[N]	48.40	59.32	94.80	158.25
		C_L/C_D	47.91	51.89	37.33	21.80

Froud number	0.211	AoA[°]	2	4	6	8
Flow Vel. [m/s]	3.988	C_L[N]	5244.13	6958.73	8048.84	7811.32
Flow Vel. [knots]	7.751	C_D[N]	104.14	128.69	206.88	353.45
		C_L/C_D	50.36	54.07	38.91	22.10

Froud number	0.281	AoA[°]	2	4	6	8
Flow Vel. [m/s]	5.315	C_L[N]	9350.73	12400.62	14401.84	13943.08
Flow Vel. [knots]	10.332	C_D[N]	179.32	223.60	359.75	624.48
		C_L/C_D	52.15	55.46	40.03	22.33

Froud number	0.326	AoA[°]	2	4	6	8
Flow Vel. [m/s]	6.174	C_L[N]	12633.98	16760.26	19483.53	18842.46
Flow Vel. [knots]	12.000	C_D[N]	238.63	298.05	481.60	840.48
		C_L/C_D	52.94	56.23	40.46	22.42

B.1.6 NACA 4418

Table B.6: CFD results of the NACA 4418 hydrofoil profile

NACA 4418		Chord Length[m]	1			
		Vessel Length[m]	36.58	g[m/s2]	9.81	

Froud number	0.140	AoA[°]	2	4	6	8
Flow Vel. [m/s]	2.658	C_L[N]	2246.22	2976.33	3664.79	4074.50
Flow Vel. [knots]	5.166	C_D[N]	52.84	61.28	75.53	96.66
		C_L/C_D	42.51	48.57	48.52	42.15

Froud number	0.211	AoA[°]	2	4	6	8
Flow Vel. [m/s]	3.988	C_L[N]	5128.93	6793.34	8396.22	9454.99
Flow Vel. [knots]	7.751	C_D[N]	112.58	131.16	161.97	208.15
		C_L/C_D	45.56	51.79	51.84	45.42

Froud number	0.281	AoA[°]	2	4	6	8
Flow Vel. [m/s]	5.315	C_L[N]	9211.17	12177.52	15086.64	17128.20
Flow Vel. [knots]	10.332	C_D[N]	192.19	225.35	279.23	359.43
		C_L/C_D	47.93	54.04	54.03	47.65

Froud number	0.326	AoA[°]	2	4	6	8
Flow Vel. [m/s]	6.174	C_L[N]	12477.20	16494.12	20457.14	23300.60
Flow Vel. [knots]	12.000	C_D[N]	254.33	298.84	370.67	477.18
		C_L/C_D	49.06	55.19	55.19	48.83

B.1.7 NACA 6418

Table B.7: CFD results of the best hydrofoil profile, the NACA 6418

NACA 6418		Chord Length[m]	1		
		Vessel Length[m]	36.58	g[m/s2]	9.81

Froud number	0.140	AoA[°]	2	4	6	8
Flow Vel. [m/s]	2.658	C_L[N]	3063.04	3780.40	4345.40	4521.92
Flow Vel. [knots]	5.166	C_D[N]	59.82	70.24	86.82	113.35
		C_L/C_D	51.20	53.82	50.05	39.89

Froud number	0.211	AoA[°]	2	4	6	8
Flow Vel. [m/s]	3.988	C_L[N]	6993.20	8646.54	10048.75	10460.06
Flow Vel. [knots]	7.751	C_D[N]	127.09	150.14	184.40	242.02
		C_L/C_D	55.03	57.59	54.49	43.22

Froud number	0.281	AoA[°]	2	4	6	8
Flow Vel. [m/s]	5.315	C_L[N]	12541.64	15524.17	18079.76	18920.44
Flow Vel. [knots]	10.332	C_D[N]	217.40	257.72	316.43	414.42
		C_L/C_D	57.69	60.24	57.14	45.66

Froud number	0.326	AoA[°]	2	4	6	8
Flow Vel. [m/s]	6.174	C_L[N]	16986.87	21040.55	24520.98	25786.03
Flow Vel. [knots]	12.000	C_D[N]	287.33	341.97	418.46	551.12
		C_L/C_D	59.12	61.53	58.60	46.79

Appendix C

Ideal Positioning Of The Stern Foil

In this appendix you can find the complete results of the 2D simulations of the stern foil on the essel, where 6 different positions were tested and compared to the baseline values of just the hull. We evaluated the hydrodynamic forces applied to the ship, more specifically the drag and lift forces, which in turn provoked a waterline change form the lower pressure zone created by the hydrofoil.

Since for this simulation configuration we had a clear distinction between the two volumes of fluid, it can be observed the significant reduction in the generated wake behind the transom of the vessel, as it as expected.

In the following images you can find represented the evolution plots of the residuals, drag and lift forces, along side the phase and dynamic pressure contours.

C.1 The 5 Testing Positions

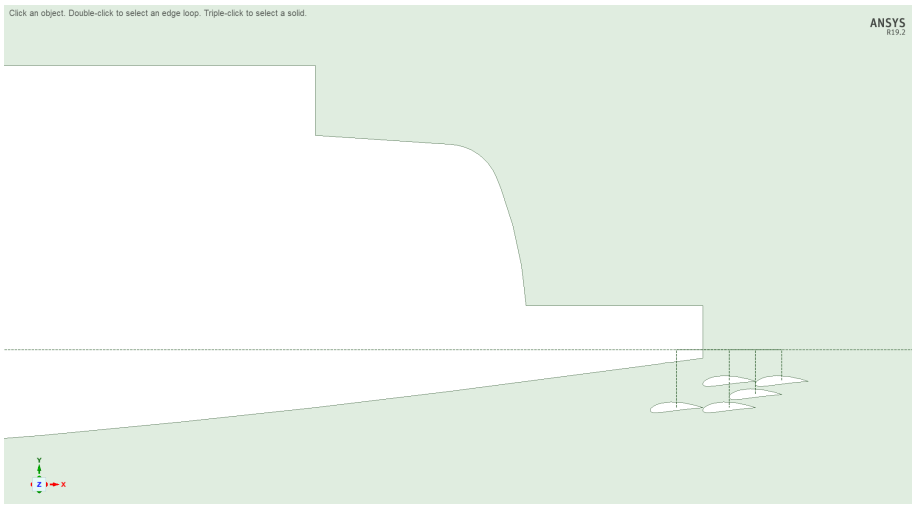

Figure C.1: The 2D representation of the stern foil positions.

C.2 Initial State

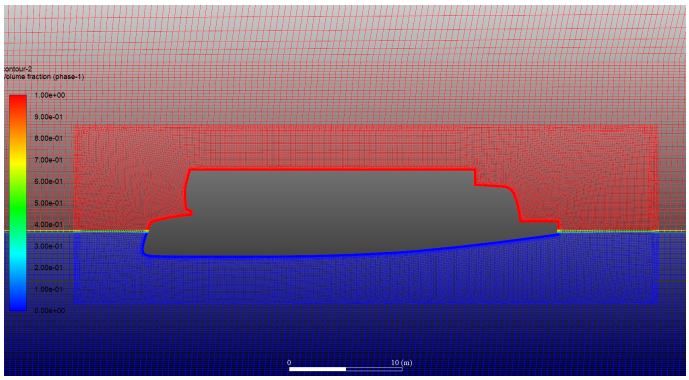

Figure C.2: 2D ship phase contour at flow velocity 0 m/s.

C.3 Baseline

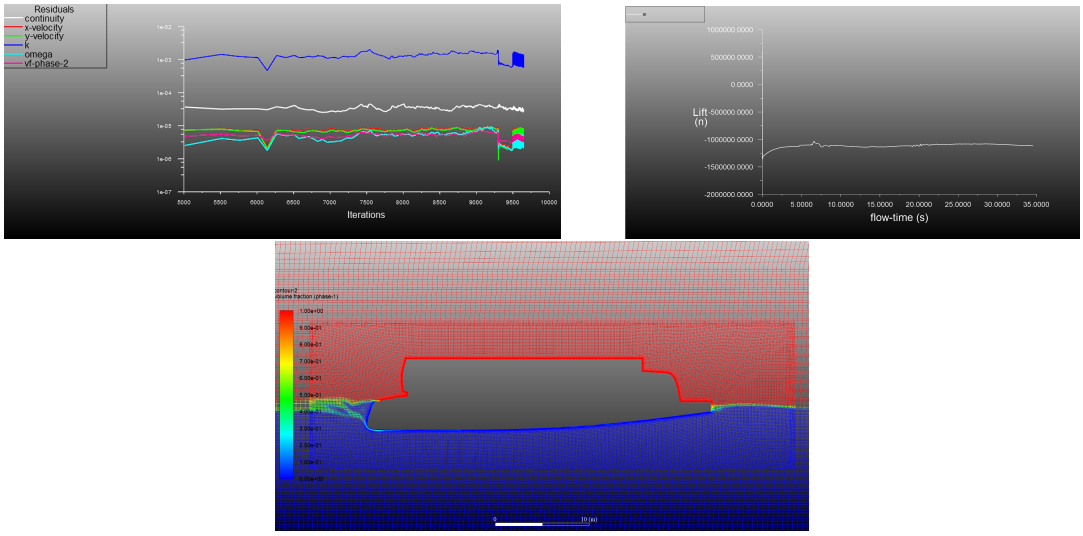

Figure C.3: 2D ship baseline simulation results, with a representation of the simulation residuals, lift force values and phase contour, respectively.

C.4 Position 1

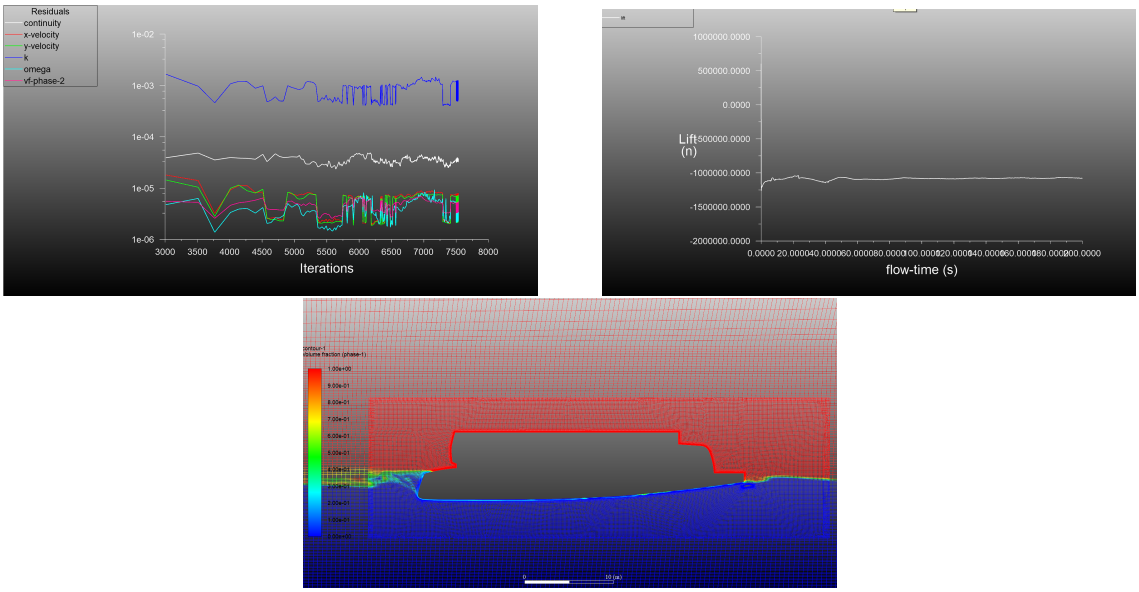

Figure C.4: 2D ship position 1 simulation results, with a representation of the simulation residuals, lift force values and phase contour, respectively.

C.5 Position 2

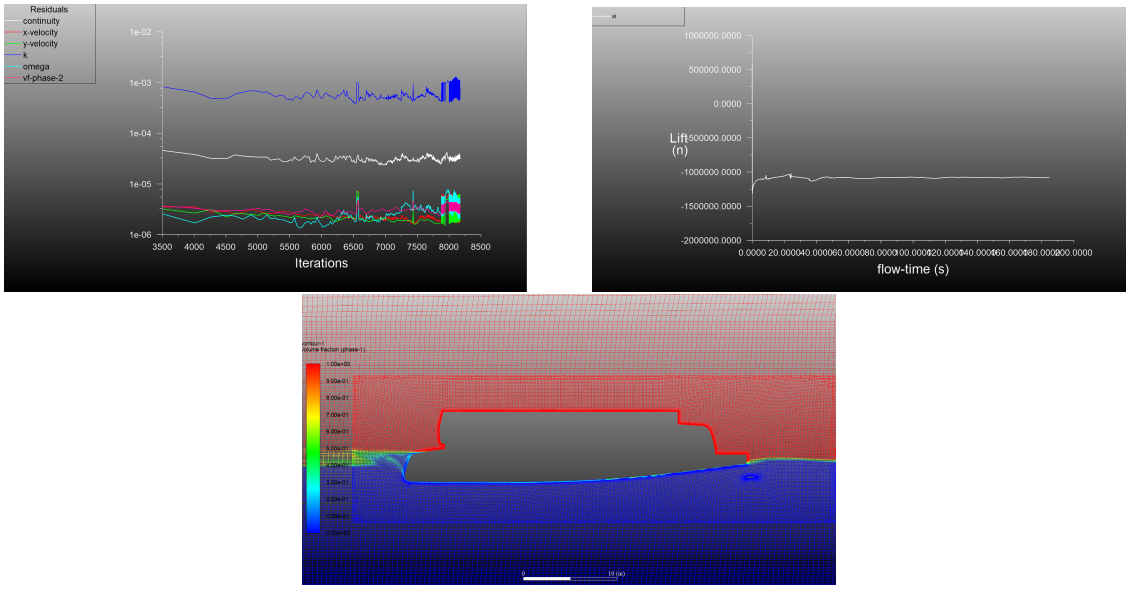

Figure C.5: 2D ship position 2 simulation results, with a representation of the simulation residuals, lift force values and phase contour, respectively.

C.6 Position 3

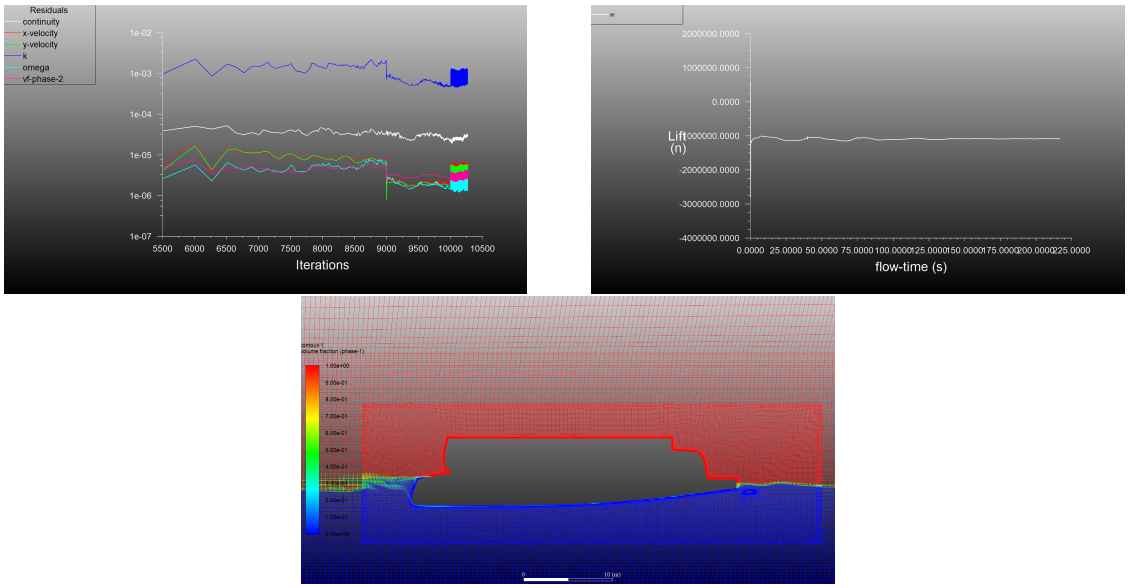

Figure C.6: 2D ship position simulation results, with a representation of the simulation residuals, lift force values and phase contour, respectively.

C.7 Position 4

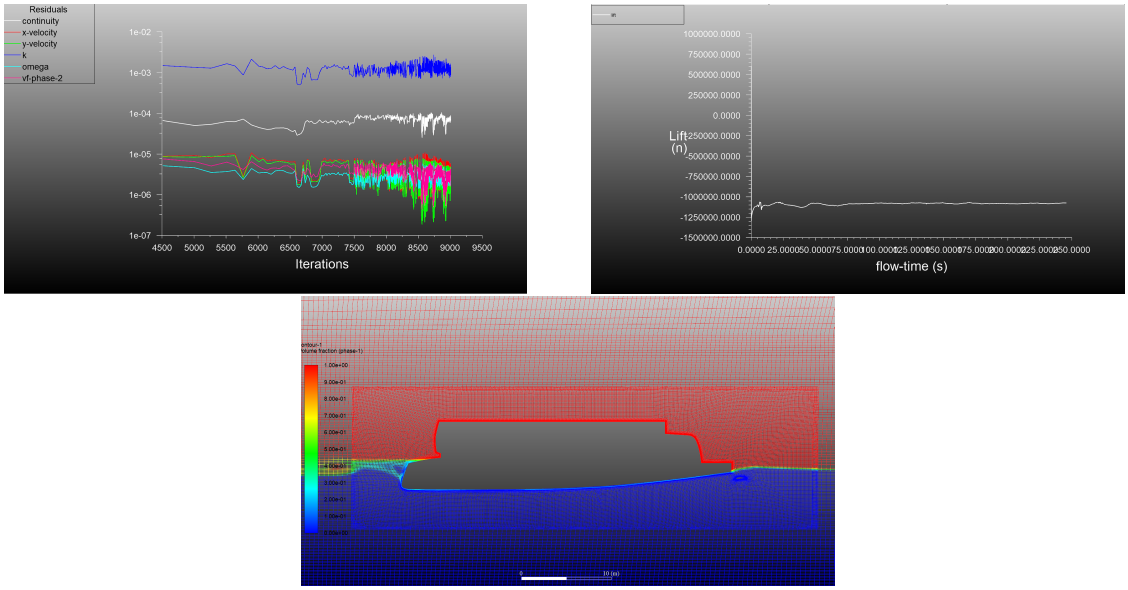

Figure C.7: 2D ship position 4 simulation results, with a representation of the simulation residuals, lift force values and phase contour, respectively.

C.8 Position 5

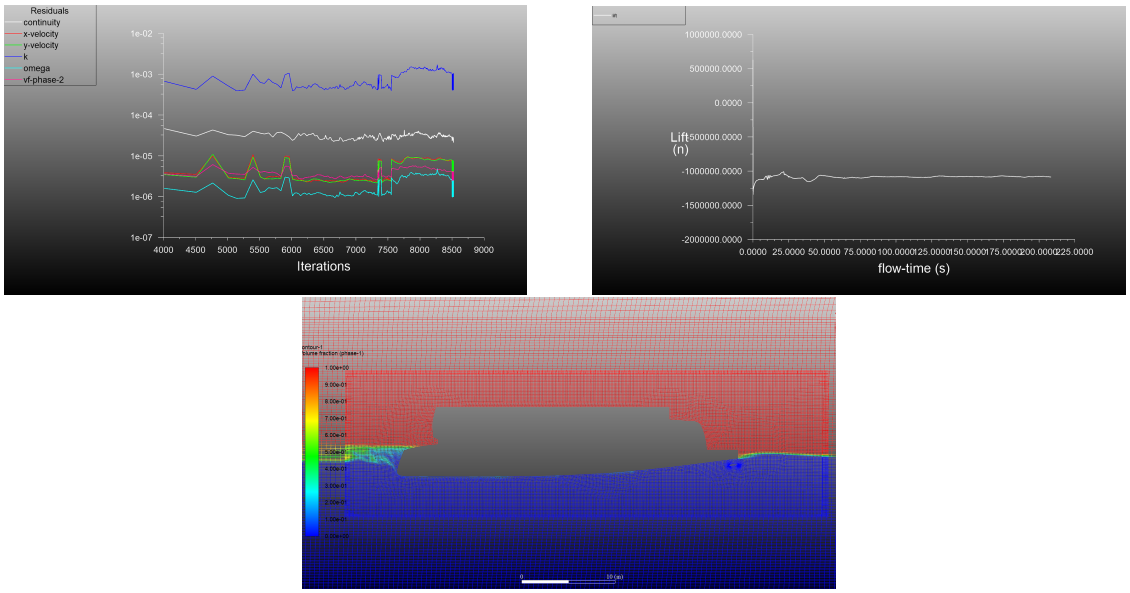

Figure C.8: 2D ship position 5 simulation results, with a representation of the simulation residuals, lift force values and phase contour, respectively.

C.9 Phase contour comparison

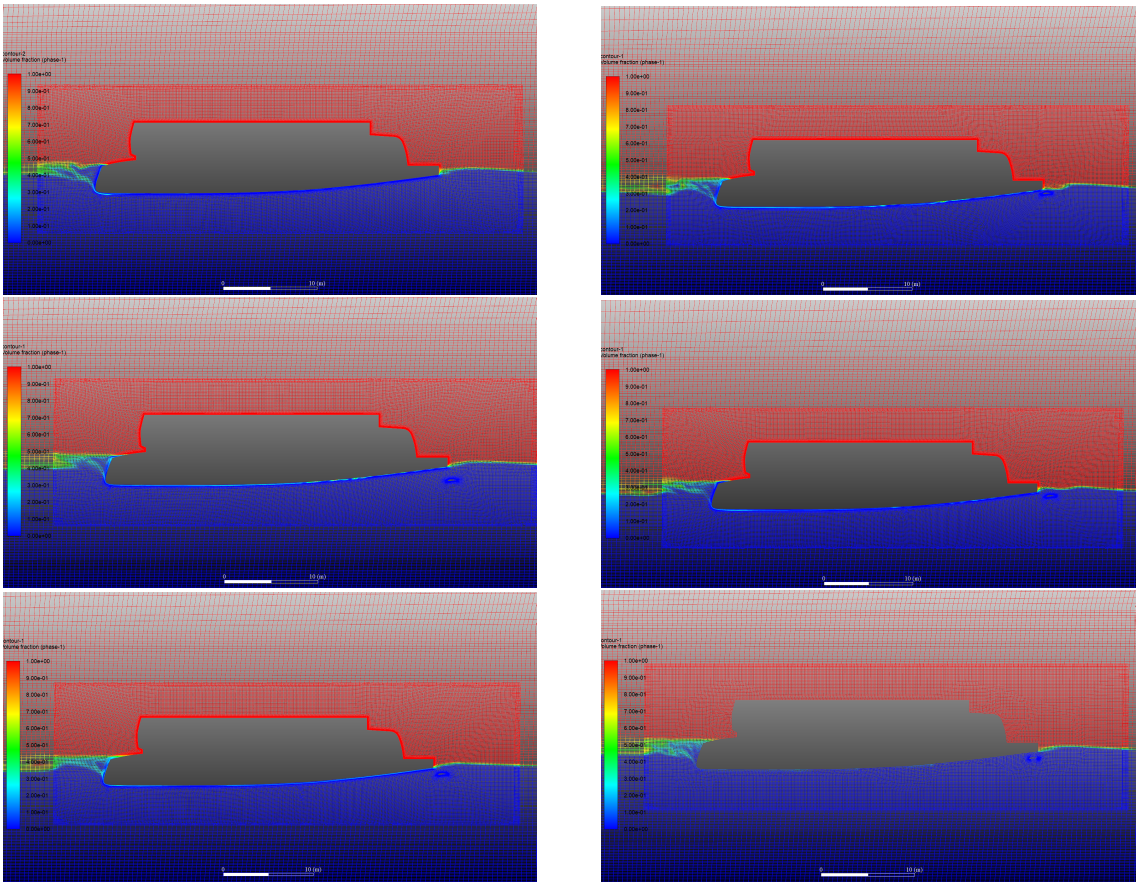

Figure C.9: Phase contour comparison between all of the different positions, here we have a representation of the baseline, position 1, position 2, position 3, position 4, position 5, respectively.

Appendix D

Numerical Methods

For this section a thorough description of the governing equations and turbulence models will be made. These equations will be describing the numerical calculations that the software *ANSYS (Fluent)* will have to perform in order to obtain the desired solutions.

In this study, we used *ANSYS (Fluent)* as a computational fluid dynamics media for multi-fluid flow. Here, the Reynolds Averaged Navier-Stokes (RANS) equation is used to represent the fluid flow and its behaviour. The RANS equation can be described as the three fundamental equations in fluid flow, the continuity equation D.1, momentum equation D.2 and the energy equation D.3. This representation was adopted from the article [13].

- Continuity Equation

$$\frac{D\rho}{Dt} + \rho \frac{\partial U_i}{\partial x_i} = 0 \tag{D.1}$$

- Momentum Equation

$$\rho \frac{\partial U_j}{\partial t} + \rho U_i \frac{\partial U_j}{\partial x_t} = \frac{\partial P}{\partial x_j} - \frac{\partial \tau_{ij}}{\partial x_i} + \rho g_j \tag{D.2}$$

- Energy Equation

$$\rho C_\mu \frac{\partial T}{\partial t} + \rho C_\mu U_i \frac{\partial T}{\partial x_i} = -P \frac{\partial U_i}{\partial x_t} + \lambda \frac{\partial^2 T}{\partial x_i^2} + \tau_{ij} \frac{\partial U_j}{\partial x_i} \tag{D.3}$$

Here, ρ, U, P, τ, and g in equation D.2 includes the density, momentum, convection surface force, diffusion and mass force. Furthermore, in equation D.3, λ and τ are the heat flux and heat transfer from mechanical energy. For the domain or enclosure , the turbulence model equation uses k-ω SST turbulence model, categorized by equation D.4 and D.5, which is generally used for this scenario, as follows:

$$\frac{\partial_{(\rho k)}}{\partial_t} + \frac{\partial_{(\rho u_j k)}}{\partial x_j} = P - \beta^* \rho \omega k + \frac{\partial}{\partial x_j}\left[\left(\mu + \sigma_k \frac{\rho k}{\omega}\right)\frac{\partial k}{\partial x_j}\right] \tag{D.4}$$

$$\frac{\partial_{(\rho k)}}{\partial_t} + \frac{\partial_{(\rho u_j \omega)}}{\partial x_j} = \frac{\gamma \omega}{k} P - \beta \rho \omega^2 + \frac{\partial}{\partial x_j}\left[\left(\mu + \sigma_\omega \frac{\rho k}{\omega}\right)\frac{\partial k}{\partial x_j}\right] + \frac{\rho \sigma_d}{\omega}\frac{\partial k}{\partial x_j}\frac{\partial \omega}{\partial x_j} \tag{D.5}$$

In these equations, β, $\beta*$, γ, σ_k and σ_d are enclosure constant coefficients. In the simulation, the model was at rest and fluids flowed towards it with a constant velocity according to the various Froude numbers specified.

The model's movement was restricted in roll, sway, surge, yaw and pitch, which basically only allowed heave movements only. To achieve them, the simulation used a User-Defined Function (UDF) for motion restrictions, as follows in the following image and equations:

```
z#include "udf.h"

DEFINE_SDOF_PROPERTIES(hull, prop, dt, time, dtime)
{

        prop[SDOF_MASS] = 260000;
        prop[SDOF_IXX] = 1221000;
        prop[SDOF_IYY] = 2452000;
        prop[SDOF_IZZ] = 3662000;
        prop[SDOF_ZERO_TRANS_X] = TRUE;
        prop[SDOF_ZERO_TRANS_Y] = TRUE;
        prop[SDOF_ZERO_TRANS_Z] = FALSE;
        prop[SDOF_ZERO_ROT_X] = TRUE;
        prop[SDOF_ZERO_ROT_Y] = FALSE;
        prop[SDOF_ZERO_ROT_Z] = TRUE;
}
```

Figure D.1: Code used for programming the degrees of freedom

$$x = x_a \cos\left(\omega_e t + \varepsilon_x \varsigma\right) = 0 \tag{D.6}$$

$$y = y_a \cos\left(\omega_e t + \varepsilon_y \varsigma\right) = 0 \tag{D.7}$$

$$z = z_a \cos\left(\omega_e t + \varepsilon_z \varsigma\right) \neq 0 \tag{D.8}$$

$$\phi = \phi_a \cos\left(\omega_e t + \varepsilon_{\phi\zeta}\right) = 0 \tag{D.9}$$

$$\theta = \theta_a \cos\left(\omega_e t + \varepsilon_\theta \varsigma\right) = 0 \tag{D.10}$$

$$\psi = \psi_a \cos\left(\omega_e t + \varepsilon_\psi \varsigma\right) = 0 \tag{D.11}$$

Here, x, y and z represent the surge, sway and heave, respectively. In addition, ϕ, θ, ψ represent the roll, pitch and yaw, respectively.

The volume of fluid (VoF) was used to generate a free surface option between fluids. A wall boundary condition was used to simulate or calculate flows near the model for the drag resistance value. Wave and turbulence values were kept low to simulate the calm water condition.

The distance for wall-flow was designed to disallow disturbance flow near the model, it is intended that the calculation of ship resistance is not affected by waves caused from outside the model. The main dimensions in the simulation were as follows [35]: The inlet boundary, located at 1-L upstream from the bow of the ship (where L is the ship's length at the water line), was defined as the inlet for fluid that equalled the ship's velocity; The outlet boundary, located at approximately 2-L downstream from the transom of the ship, was also defined as the inlet boundary but at a constant pressure, which allowed incompressible flow in the scheme. Moreover, the bottom and top walls were located at 1-L from the keel and 0.25-L from the deck, respectively. In addition, the side wall was located at 1-L from the longitudinal axis. The dimensions of the simulation are determined based on the practical guidelines of the International Towing Tank Conference, [35].

References

[1] Silent-Yachts. Silent-yachts, 2022. Accessed on 22 6, 2023.

[2] Matthew J. Page; Joanne E. McKenzie; Patrick M. Bossuyt; Isabelle Boutron; Tammy C. Hoffmann; Cynthia D. Mulrow; et all. The prisma 2020 statement: an updated guideline for reporting systematic reviews. *RESEARCH METHODS AND REPORTING*, pages 1–9, January 2020.

[3] Gabriel T. Fonteles Richard D. Schachter. Preliminary design dimensioning of hydrofoil boats with fully submerged and surface piercing foils. *Sociedade Brasileira de Engenharia Naval*, pages 1–17, March 2022.

[4] Hull Vane B.V. Hull vane, 2022. Accessed on 27 6, 2023.

[5] K. Uithof; P. van Oossanen; N. Moerke; P.G. van Oossanen and K.S. Zaaijer. An update on the development of the hull vane. *Elsevier - Engineering Village*, pages 1–11, April 2023.

[6] Juri Karinen. Hybrid catamaran, 2021. Accessed on 27 6, 2023.

[7] Dan Yang Taiba Kouser1, Yongliang Xiong and Sai Peng. Numerical study on drag reduction and wake modification for the flows over a hydrofoil in presence of surface heterogeneity. *Advances in Mechanical Engineering*, pages 1–14, January 2022.

[8] Anirban Bhattacharyya Rajni Kant. Hydrofoil geometry and leading-edge modifications: Influence of section profile, aspect ratio, and sweep. *Ocean Engineering*, pages 1–22, August 2022.

[9] Aevelina Rahmanc Md. Ariful Hoquea, Md. Mashud Karimb. Simulation of water wave generated by shallowly submerged asymmetric hydrofoil. *Elsevier Ltd*, pages 1–6, March 2017.

[10] Moloud Arian Maram; Hamid Reza Ghafari; Hassan Ghassemi; and Mahmoud Ghiasi. Numerical study on the tandem submerged hydrofoils using rans solver. *Department of Maritime Engineering*, pages 1–17, February 2021.

[11] Muhammad Aziz Murdianto; Muhammad Arif Budiyanto; Muhamad Fuad Syahrudin. Application of stern foil on full draft patrol vessel at high speed condition using computational fluid dynamics (cfd) method. *AIP Conference Proceedings 2255, 020023*, pages 1–7, September 2020.

[12] Naufal Yudha Prawira; Mohamad Arif Andira; Muhammad Arif Budiyanto. The effect of depth variations of stern foil on high speed craft with computational fluid dynamics method. *AIP Conference Proceedings 2255, 020023*, pages 1–8, September 2021.

[13] Muhamad Fuad Syahrudin Muhammad Arif Budiyanto and Muhammad Aziz Murdianto. Investigation of the effectiveness of a stern foil on a patrol boat by experiment and simulation. *Taylor And Francis*, pages 1–17, January 2020.

[14] Srijna Singh; Mohammad Danish; Kaushik Saha; Baij Nath Singh. Numerical simulation and analysis of fluid-structure interaction on 3d mhkf-180 and naca4418 cavitating hydrofoils. *Ocean Engineering*, pages 1–16, February 2023.

[15] Bruno Bouckaert. An underwater spoiler on a warship: Why, when and how? *SCIENTIFIC JOURNAL OF POLISH NAVAL ACADEMY*, pages 1–19, April 2018.

[16] Kiryanto. Analysis of the effect of hull vane on ship resistance using cfd methods. *Earth and Environmental Science*, pages 1–9, April 2021.

[17] K. Uithof; N. Hagemeister; B. Bouckaert; P. G. van Oossanen; and N. Moerke. A systematic comparison of the influence of the hull vane, interceptors, trim wedges, and ballasting on the performace of the 50m amecrc series #13 patrol vessel. *Advanced Technologies in Naval Design, Construction and Operation*, pages 1–8, June 2016.

[18] K. Uithof; B. Bouckaert; P. G. van Oossanen; and N. Moerke. Hull vane® on 108m holland-class opvs: Effects on fuel consumption and seakeeping. *Advanced Technologies in Naval Design, Construction and Operation*, pages 1–8, June 2016.

[19] K Suastika and Apriansyah. Effects of stern-foil submerged elevation on the lift and drag of a hydrofoil craft. *Earth and Environmental Science*, pages 1–9, April 2018.

[20] N. Hagemeister; K. Uithof; B. Bouckaert; Andrea Mikelic. Hull vane® versus lengthening. *FAST2017*, pages 1–11, January 2017.

[21] Yingqian Liao ; Anil Yildirim ; Joaquim R.R.A. Martins ; Yin Lu Young. Rans-based optimization of a t-shaped hydrofoil considering junction design. *Elsevier*, pages 1–25, July 2022.

[22] YCihad Çelik; Devrim Bülent Danış¸man; Shahroz Khan; Panagiotis Kaklis. A reduced order data-driven method for resistance prediction and shape optimization of hull vane. *Elsevier*, pages 1–17, July 2021.

[23] Hongbo Hou; Mateusz Krajewski; Kaan Ilter; Sandy Day; Mehmet Atlar; Weichao Shi. An experimental investigation of the impact of retrofitting an underwater stern foil on the resistance and motion. *Elsevier*, pages 1–17, April 2020.

[24] P.A.P. Souza; P.I.D. Lameira; H.P. Picanço; H.B. Moraes ; L.C.P. Campos Filho. Hydrofoil profile numerical analysis for low reynolds number. *Developments in Maritime Technology and Engineering*, pages 1–9, March 2021.

[25] Tsung-chow Su Zao Ni, Manhar Dhanak. Performance of a hydrofoil operating close to a free surface over a range of angles of attack. *International Journal of Naval Architecture and Ocean Engineering*, pages 1–11, January 2021.

[26] Valerio Ruggiero Antonio Giallanza1, Giuseppe Marannano1 · Ferdinando Morace. Numerical and experimental analysis of a high innovative hydrofoil. *International Journal on Interactive Design and Manufacturing*, pages 1–15, November 2019.

[27] Gabriel T. Fonteles Richard D. Schachter. Preliminary design dimensioning of hydrofoil boats with fully submerged and surface piercing foils. *International Journal on Interactive Design and Manufacturing*, pages 1–17, March 2022.

[28] Parikshit Kundu. Effects of circular trailing edge with the dimple on flow separation of naca s1210 hydrofoil. *Journal of MECHANICAL ENGINEERING SCIENCE*, pages 1–14, March 2020.

[29] Hassan Ghassemi Amin Najafia, Hashem Nowruzia. Performance prediction of hydrofoil-supported catamarans using experiment and anns. *Elsevier Ltd*, pages 1–19, April 2018.

[30] Youhei Takagi Chota Terui, Takanori Hino. Numerical analysis of wake wash reduction for catamaran with hydrofoils. *Elsevier Ltd*, pages 1–14, April 2023.

[31] Taghi Aliakbari Amin Najafi and Seyed Abolfazl Hashemi. Experimental optimization of hydrodynamic performance of catamarans using hydrofoil element. *Journal of ENGINEERING FOR THE MARITIME ENVIRONMENT*, pages 1–14, January 2018.

[32] Gilberto Osorio-Gómez Erick Giraldo-Pérez, Esteban Betancur. Experimental and statistical analysis of the hydrodynamic performance of planing boats: A comparative study. *Ocean Engineering*, pages 1–14, January 2018.

[33] NA. Tutorial: Heave and pitch simulation of ship hull moving through head sea waves. *NA*, pages 1–13, February 2011.

[34] K. Ward E. Jacobs and R. Pinkerton. Report no. 460: The characteristics of 78 related airfoil sections from tests in the variable-density wind tunnel. *National Advisory Committee For Aeronautics*, pages 1–61, November 1935.

[35] NA. Ittc – recommended procedures and guidelines. *Practical Guidelines for Ship CFD Applications*, pages 1–18, September 2011.

[36] Airfoil Tools. Airfoil tools, 2022. Accessed on 22 6, 2023.